Plasma abatement of perfluorocompounds in inductively coupled plasma reactors

Xudong "Peter" Xu,[a] Shahid Rauf,[b] and Mark J. Kushner[c]
University of Illinois, Department of Electrical and Computer Engineering, Urbana, Illinois 61801

(Received 13 May 1999; accepted 1 October 1999)

Perfluorinated compounds (PFCs), gases which have large global warming potentials, are widely used in plasma processing for etching and chamber cleaning. Due to underutilization of the feedstock gases or by-product generation, the effluents from plasma tools using these gases typically have large mole fractions of PFCs. The use of plasma burn-boxes located downstream of the plasma chamber has been proposed as a method for abating PFC emissions with the goals of reducing the cost of PFC abatement and avoiding the NO_x formation usually found with thermal treatment methods. Results from the two-dimensional Hybrid Plasma Equipment Model have been used to investigate the scaling of plasma abatement of PFCs using plasma burn-boxes. An inductively coupled plasma (ICP) etching chamber is modeled to determine the utilization of the feedstock gases and the generation of by-products. The effluent from the etching chamber is then passed through a plasma burn-box excited by a second ICP source. O_2, H_2, and H_2O are examined as additive gases in the burn-box. We find that C_2F_6 (or CF_4) consumption in the etching reactor increases with increasing ICP power deposition at constant C_2F_6 (or CF_4) mole fraction, and decreasing C_2F_6 (or CF_4) mole fraction or total gas flow rate at constant power. The efficiency of removal of C_2F_6 (eV/molecule), however, is strongly dependent only on the C_2F_6 mole fraction and total gas flow rate. All PFCs in the effluent can generally be abated in the burn-box at high power deposition with a sufficiently large flow of additive gases. In general CF_4 generation occurs during abatement of C_2F_6 using O_2 as an additive. CF_4 is not, however, substantially produced when using H_2 or H_2O as additives. The efficiency of PFC abatement decreases with increasing power and decreasing additive mole fraction. © *2000 American Vacuum Society.* [S0734-2101(00)02401-5]

I. INTRODUCTION

Perfluorocompound (PFC) gases, such as C_2F_6 and CF_4, are commonly used in the semiconductor industry for plasma etching and chamber cleaning.[1–4] The use of these gases is being reassessed by the semiconductor industry because they have long atmospheric lifetimes, are strong infrared absorbers, and so have large global warming potential. The Environmental Protection Agency (EPA) and individual semiconductor companies signed memoranda of understanding in March 1996 in an effort to reduce PFC emissions. There are four generally accepted approaches to reducing PFC emission; process optimization, substitution, recycling and recovery, and abatement.[5] There have been significant efforts to optimize etching and cleaning processes to increase PFC utilization and decrease emissions. However, it has been difficult for process optimization to achieve the desired reductions in PFC emissions without detrimentally affecting product throughput, especially in plasma etching. Though some alternative chemicals (C_3F_8 and NF_3)[5,6] show promise as substitutes, they also have high global warming potentials and may result in PFC by-product generation. Recycling and recovery of unreacted PFCs from the effluent may be desirable from a PFC utilization standpoint, however, current recovery technologies are not economic for existing fabrication facilities.

Plasma remediation of gas emissions from plasma and thermal reactors is an attractive alternative abatement strategy. A typical plasma abatement device consists of a reactor with a radio frequency (rf) or microwave plasma generating system placed downstream of the etching chamber's turbomolecular pump. These plasma abatement systems can be applied locally to a single semiconductor manufacturing tool or reactor, and so can be specialized to the needs of a particular tool or be retrofitted to existing tools. Efficient destruction of C_2F_6 in reactor effluents using plasma abatement systems has been experimentally demonstrated in a variety of low pressure devices. For example, Mohindra *et al.*[7] investigated C_2F_6 abatement using a microwave tubular reactor. While varying total flowrate (400–1200 sccm), power (300–700 W), and pressure (4–8 Torr) for a gas mixture of $C_2F_6/O_2=50/50$, they obtained nearly 100% abatement of C_2F_6 at low flowrates and high powers. They also investigated the abatement of CF_4, SF_6, and CHF_3. Hartz and co-workers[8] investigated low-pressure surface wave plasmas to abate C_2F_6, and found that when using only O_2 as an additive gas there was a significant amount of CF_4 produced. CF_4 mole fractions in the exhaust were 0.002–0.145 (for pressures of 2.5–5.3 Torr) depending upon the C_2F_6/O_2 ratio. At a microwave power deposition of 1950 W, they found that a C_2F_6/O_2 ratio of 1/3 had the highest destruction effi-

[a]Present address: LSI Logic, 3115 Alfred St., Santa Clara, CA 95054.
[b]Present address: Motorola, 3501 Ed Bluestein Blvd., MD K-10, Austin, TX 78721; electronic mail: ra8952@email.sps.mot.com
[c]Author to whom correspondence should be addressed; electronic mail: mjk@uiuc.edu

ciency (98.1%) with the lowest CF_4 production (0.64%). They also demonstrated that the addition of natural gas (consisting of mostly CH_4 and C_2H_6) could impede CF_4 generation.

An rf plasma system for abatement of C_2F_6 was investigated by Sawin and Vitale.[9] Their reactor had a 1.2 ℓ volume and 10 cm diameter with an internal coil. They also showed that C_2F_6 can be abated with an oxygen additive, but that CF_4 production was significant. A modeling study by Fiala *et al.*[10] of abatement of a $C_2F_6/O_2=40/60$ mixture using an inductively coupled plasma (ICP) also showed that CF_4 can be generated in significant proportions. A commercial point-of-use rf abatement system developed by Litmas was investigated by Tonnis *et al.*[11] They measured the destruction and removal efficiency of PFCs for process gas mixtures using $CHF_3/Ar/CF_4$. For example, in a mixture of $CHF_3/Ar/CF_4=10/12/1$ at a flow rate of 115 sccm with 70 sccm O_2 as an additive and a power of 1050 W, CF_4 was abated with an efficiency of 96%, while the CHF_3 destruction was 99.5%. Using 250 sccm of H_2O as an additive produced destruction efficiencies of 99.6% for CF_4 and 98.6% for CHF_3.

The products of plasma abatement of PFCs are typically COF, COF_2, CO, CO_2, HF, F_2, and F. These oxidation products can usually be remediated by conventional means. For example, COF_2 is easily removed by processing the gas stream through a water bubbler or water spray. This method is also effective at removing F and F_2. CO can be converted to CO_2 using a platinum catalyst. Thermal systems are now often used to remediate PFCs from processing effluents. Thermal abatement is usually performed after the roughing pump where the exhaust stream is diluted with N_2. As a result, thermal systems can produce by-products such as NO and NO_2. Plasma abatement systems, located between the turbo and roughing pumps, operate at intermediate pressures (100 s mTorr) in the absence of N_2, and so typically do not generate NO_x.

In this article, the dissociation of PFCs in an ICP etching reactor and their subsequent remediation in a downstream plasma burn-box will be discussed using results from a two-dimensional computer model. We found that C_2F_6 (or CF_4) consumption in the etching reactor increases with increasing ICP power deposition at fixed PFC mole fraction, and decreasing C_2F_6 (or CF_4) mole fraction or total gas flow rate at constant power. The efficiency of destruction of C_2F_6 (eV molecule), however, is strongly dependent only on the C_2F_6 mole fraction and total gas flow rate. The effluents can be abated in the burn-box at high power with sufficiently large flow of additive gases, such as O_2, H_2, or H_2O. The energy efficiency of abatement (as measured by eV/molecule) decreases with increasing power and decreasing additive mole fraction.

The computational platform used in this study is described in Sec. II. The general plasma characteristics, and consumption and generation of PFCs in the plasma etching chamber are discussed in Sec. III. Abatement of the effluents in a plasma burn-box is discussed in Sec. IV. Our concluding remarks are in Sec. V.

II. DESCRIPTION OF THE MODEL

The model used in this study is the two-dimensional Hybrid Plasma Equipment Model (HPEM). The HPEM has been previously described in Refs. 12 and 13 (and references therein) and so will be only briefly discussed here. The 2D HPEM is a (r, z) cylindrically symmetric simulation which consists of three main modules; the electromagnetic module (EMM), the electron energy transport module (EETM), and the fluid-kinetics module (FKM). The EMM calculates the electric and magnetic fields in the reactor which are inductively coupled from transformer coils. These fields are used in the EETM to generate the electron temperature, transport coefficients and electron impact source functions. These values are then passed to the FKM. In the FKM, continuity, momentum, and energy equations for all neutral and charged densities are integrated, and Poisson's equation is solved for the electric potential. The plasma conductivity produced in FKM is passed to the EMM, and the species densities, fluxes, and power deposition are transferred to the EETM. The modules are iterated until cycle averaged plasma and neutral densities converge. Acceleration algorithms are used to speed the rate of convergence of the model.

As an improvement to the previously described HPEM, energy equations for all heavy neutral and charged species have been integrated into the FKM to obtain the ion and neutral temperatures. For electrically neutral species, the energy equation is

$$\frac{\partial N_i \epsilon_i}{\partial t} + \nabla \cdot \mathbf{Q}_i + P_i \nabla \cdot \mathbf{U}_i + \nabla \cdot (N_i \mathbf{U}_i \epsilon_i) = \sum_j 3 \frac{m_{ij}}{m_i + m_j} N_i N_j R_{ij} k_B (T_j - T_i) \pm \sum_j 3 N_i N_j R_{ij} k_B T_j, \quad (1)$$

where N_i, $\mathbf{U}_i$, ϵ_i, T_i, $\mathbf{Q}_i$, P_i, and m_i are, respectively, the number density, mean velocity, thermal energy, temperature, thermal flux, pressure, and mass of species *i*. R_{ij} is the rate constant for the collision between species *i* and *j*, $m_{ij} \equiv m_i m_j/(m_i + m_j)$ is the reduced mass and k_B is Boltzmann's constant. The first sum on the RHS is for elastic collisions where Lennard-Jones parameters were used to compute the rate coefficients.[14] The second sum accounts for identity changing charge exchange collisions where the contribution is positive or negative, depending on whether the neutral particle is being generated or destroyed. Other quantities in Eq. (1) are

$$\epsilon_i = c_v T_i, \quad P_i = N_i k_B T_i, \quad \mathbf{Q}_i = -\kappa_i \nabla T_i, \quad (2)$$

where c_v and κ_i are, respectively, the specific heat at constant volume and thermal conductivity for species *i*. The thermal conductivity was obtained from[15]

$$\kappa_i = k_B N_i \left(\frac{8k_B T_i}{\pi m_i}\right)^{1/2} \left[\sum_j 2N_j \sigma_{ij}(m_{ij}/m_i)^{1/2}\right]^{-1}, \tag{3}$$

where σ_{ij} is the Lennard-Jones collision cross section for species i and j. The rate constants R_{ij} in Eq. (1) for elastic collisions are

$$R_{ij} = \left(\frac{8k_B T_{\text{eff}}}{\pi m_{ij}}\right)^{1/2} \sigma_{ij}, \tag{4}$$

where $T_{\text{eff}} \equiv T_i + m_{ij}(\boldsymbol{\nu}_i - \boldsymbol{\nu}_j)^2/3k_B$ is the effective temperature which takes account of the directed motion of the particles. Rate constants for charge exchange reactions are specified in the reaction mechanism while those for electron impact momentum transfer are obtained from the EETM.

In addition to the processes included in Eq. (1), the electromagnetic and electrostatic fields also contribute to the ion energy. Taking into account the additional heating resulting from these fields, the ion energy conservation relation is

$$\frac{\partial N_i \epsilon_i}{\partial t} + \nabla \cdot \mathbf{Q}_i + P_i \nabla \cdot \mathbf{U}_i + \nabla \cdot (N_i \mathbf{U}_i \epsilon_i) = \frac{N_i q_i^2 \nu_i}{m_i(\nu_i^2 + \omega^2)} E^2 + \frac{N_i q_i^2}{m_i \nu_i} E_s^2 + \sum_j 3 \frac{m_{ij}}{m_i + m_j} N_i N_j R_{ij} k_B (T_j - T_i), \tag{5}$$

where ν_i, ω, E, and E_s are, respectively, the momentum transfer collision frequency of species i, radian frequency and the magnitude of the azimuthal inductive, and static electric fields. The first and second term on the right-hand side of Eq. (5), respectively, account for heating due to acceleration in the electromagnetic and electrostatic fields.

At sufficiently high pressures, gas atoms come into thermal equilibrium with surfaces they come in contact with. The gas and surface temperature are, therefore, essentially the same at the interface. However, at low pressures there might not be sufficient collisions to efficiently couple the gas and adjacent surfaces resulting in their having different temperatures. This condition is known as the temperature jump effect.[16–18] Since ICPs are generally operated at low pressures (<10s mTorr), a temperature jump at reactor walls is accounted for using the method developed by Kennard.[16] Using this method, the difference between the wall temperature T_w and the gas temperature T_g at the wall are given by

$$T_w - T_g = g \frac{\partial T_g}{\partial x}. \tag{6}$$

The temperature T_g and its derivative are computed at the wall. The factor g is

$$g = \frac{(2-\alpha)(9\gamma - 5)}{2\alpha(\gamma+1)} \lambda, \tag{7}$$

where α, γ, and λ are, respectively, the accommodation coefficient, ratio of specific heats, and mean free path. The accommodation coefficient determines how well the gas thermally couples to the surface and its value varies from 0 (no coupling) to 1 (perfect coupling). The actual value depends on the gas, condition of the surface, and temperature, typically decreasing with increasing temperature. Typical accommodation coefficients vary from, for example, 0.1 for H_2 on Pt to 0.9 for Ne on W.[19] An accommodation coefficient of 0.35 was used in this work. Slip boundary conditions were employed using the method described by Thompson.[20]

In the HPEM, continuity and momentum conservation equations are solved by discretizing the equations in space and time, starting with initial conditions and marching forward in time until a steady-state solution is obtained. It was found, however, that the time required for particle energies to attain steady state is significantly longer than other plasma time scales. To expedite the simulation, we therefore solved the steady-state versions of Eqs. (1) and (5) (with time derivatives set equal to zero) on every iteration through the HPEM using a successive-over-relaxation technique. The average gas temperature, which is a density weighed average of neutral species, is then used for chemical reactions which are dependent on temperature. We specify a pressure and a fixed input flowrate (sccm) for the flow boundary conditions. The output pump speed is adjusted to maintain the desired pressure and a constant mass flux through the reactor.

In this work, we are investigating ICPs sustained in Ar/C_2F_6 and Ar/CF_4 mixtures in a low-pressure plasma (10 mTorr) etching reactor, and discharges in their effluents mixed with O_2, H_2, or H_2O in a higher pressure (150 mTorr) plasma burn-box. The species and reactions included for the low- and high-pressure reactors are listed in Table I for $Ar/CF_4/C_2F_6$ and Table II for $Ar/CF_4/C_2F_6/O_2/H_2O/H_2$. The reaction mechanism for the burn-box also contains the reactions listed in Table I with the exception that some reaction rates are dependent on the gas pressure. All pertinent electron impact reactions, such as vibrational excitation, are included in the electron kinetics and in the calculation of electron energy distributions and transport. We have not, however, explicitly included vibrationally excited states as separate gas phase species in the model. Although heavy particle reaction rate coefficients can be a function of the vibrational state of the reactant, vibrationally dependent reaction rate coefficients are not generally available for these chemistries and so were not included. Radiation transport was not explicitly included in the model other than by radiative relaxation of excited states. The media is therefore assumed to be optically thin.

Boundary conditions for neutral and charged species striking materials are obtained by specifying reaction probabilities on the surface and product species returning to the plasma. Reactive sticking coefficients and returning products used here are shown in Table III. All ions are assumed to have unity probability for neutralization prior to returning to the plasma. Many of these wall reactions represent our best estimates, in the absence of supporting experimental data. Significant differences in reactivities on surfaces, particularly in the burn-box, could produce systematic differences in our results. We parameterized key reactive sticking coefficients to determine their effects, and those results will be discussed elsewhere.

TABLE I. $Ar/CF_4/C_2F_6$ reaction mechanism.[a] Species: Ar, Ar*, Ar^+, CF_4, CF_3^+, CF_3^-, CF_2, F, F^-, F_2, C_2F_6, C_2F_5, C_2F_4, C_2F_3, SiF_2, e.

Reaction	Rate coefficient[b]	Reference	Reaction	Rate coefficient[b]	Reference
$e+Ar \rightarrow Ar^* + e$	c	21	$Ar^*+CF_2 \rightarrow CF+F+Ar$	4.0×10^{-11}	30
$e+Ar \rightarrow Ar^+ + e + e$	c	22	$Ar^*+C_2F_5 \rightarrow CF_2+CF_3+Ar$	4.0×10^{-11}	30
$e+Ar^* \rightarrow Ar^+ + e + e$	c	23	$Ar^*+C_2F_3 \rightarrow CF_2+CF+Ar$	4.0×10^{-11}	30
$e+Ar^* \rightarrow Ar + e$	c	23	$Ar^*+C_2F_6 \rightarrow CF_3+CF_3+Ar$	4.0×10^{-11}	30
$e+CF_4 \rightarrow CF_3+F^-$	c	24	$Ar^*+C_2F_4 \rightarrow CF_2+CF_2+Ar$	4.0×10^{-11}	30
$e+CF_4 \rightarrow CF_3^-+F$	c	24	$CF_3^++CF_3 \rightarrow CF_3^++CF_3$	1.0×10^{-9}	27
$e+CF_4 \rightarrow CF_3+F+e$	c	24	$CF_3^++C_2F_6 \rightarrow C_2F_5^++CF_4$	3.50×10^{-11}	27
$e+CF_4 \rightarrow CF_3^++F+e+e$	c	24	$C_2F_5^++C_2F_5 \rightarrow C_2F_5^++C_2F_5$	1.0×10^{-9}	27
$e+CF_4 \rightarrow CF_2+F+F+e$	c	24	$C_2F_4^++C_2F_4 \rightarrow C_2F_4^++C_2F_4$	1.0×10^{-9}	27
$e+CF_3 \rightarrow CF_2+F+e$	c	24[d]	$F^-+Ar^+ \rightarrow F+Ar$	1.0×10^{-7}	31
$e+CF_3 \rightarrow CF_2+F^-$	c	24[d]	$F^-+CF_3^+ \rightarrow F+CF_3$	1.0×10^{-7}	31
$e+C_2F_6 \rightarrow CF_3^++CF_3+e+e$	c	25	$F^-+C_2F_4^+ \rightarrow F+C_2F_4$	1.0×10^{-7}	31
$e+C_2F_6 \rightarrow CF_3+CF_3^-$	c	25	$F^-+C_2F_5^+ \rightarrow F+C_2F_5$	1.0×10^{-7}	31
$e+C_2F_6 \rightarrow C_2F_5+F^-$	c	25	$CF_3^-+Ar^+ \rightarrow CF_3+Ar$	1.0×10^{-7}	31
$e+C_2F_6 \rightarrow CF_3+CF_3+e$	c	25	$CF_3^-+CF_3^+ \rightarrow CF_3+CF_3$	1.0×10^{-7}	31
$e+C_2F_6 \rightarrow CF_2+CF_3+e$	c	25	$CF_3^-+C_2F_4^+ \rightarrow CF_3+C_2F_4$	1.0×10^{-7}	31
$e+C_2F_4 \rightarrow CF_2+CF_2+e$	c	25[e]	$CF_3^-+C_2F_5^+ \rightarrow CF_3+C_2F_5$	1.0×10^{-7}	31
$e+C_2F_4 \rightarrow C_2F_4^++e+e$	c	25[e]	$CF_3^-+F \rightarrow CF_3+F^-$	5.0×10^{-8}	31
$e+C_2F_4 \rightarrow F^-+C_2F_3$	c	25	$F+F+M \rightarrow F_2+M$	$2.4\times10^{-33}(T/298)^{0.033}$ $cm^6\,s^{-1}$	32
$e+CF_3^+ \rightarrow CF_2+F$	2.0×10^{-8}	26[f]	$F+C_2F_4 \rightarrow CF_3+CF_2$	4.0×10^{-11}	33
$e+C_2F_5^+ \rightarrow CF_3+CF_2$	2.0×10^{-8}	26[f]	$F+C_2F_5 \rightarrow CF_3+CF_3$	1.0×10^{-11}	33
$e+C_2F_4^+ \rightarrow CF_2+CF_2$	2.0×10^{-8}	26[f]	$F+C_2F_3 \rightarrow C_2F_4$	1.0×10^{-12}	34
$Ar^++Ar \rightarrow Ar+Ar^+$	1.0×10^{-9}	27	$F+CF_3 \rightarrow CF_4$	$1.99\times10^{-10}(T/300)^{-7.71}$ $\exp(-1183.4/T)$	35
$Ar^++CF_4 \rightarrow CF_3^++F+Ar$	7.0×10^{-10}	27	$F+CF_2 \rightarrow CF_3$	8.40×10^{-15}	33
$Ar^++CF_3 \rightarrow CF_3^++Ar$	7.0×10^{-10}	27	$F_2+CF_2 \rightarrow CF_3+F$	4.56×10^{-13}	34
$Ar^++C_2F_6 \rightarrow CF_3^++CF_3+Ar$	9.58×10^{-10}	27	$F_2+CF_3 \rightarrow CF_4+F$	1.88×10^{-14}	34
$Ar^++C_2F_5 \rightarrow C_2F_5^++Ar$	1.0×10^{-10}	28[f]	$CF_3+CF_3 \rightarrow C_2F_6$	7.67×10^{-12}	34
$Ar^++C_2F_4 \rightarrow C_2F_4^++Ar$	1.0×10^{-10}	28[f]	$CF_2+CF_2 \rightarrow C_2F_4$	5.0×10^{-14}	34
$Ar^*+Ar^* \rightarrow Ar^++Ar+e$	5.0×10^{-10}	29	$CF_2+CF_3 \rightarrow C_2F_5$	8.26×10^{-13}	34
$Ar^*+CF_4 \rightarrow CF_2+F_2+Ar$	4.0×10^{-11}	30			
$Ar^*+CF_3 \rightarrow CF_2+F+Ar$	4.0×10^{-11}	30			

[a]Only reactions directly affecting species densities are shown here. Additional electron impact collisions (e.g., momentum transfer, vibrational excitation) are included in the EETM.
[b]Rate coefficients have units $cm^3\,s^{-1}$ unless noted otherwise.
[c]Computed using the electron energy distribution and electron impact cross section from cited reference.
[d]Estimated by analogy to CF_4.
[e]Estimated by analogy to C_2F_6.
[f]Estimated. See cited reference for similar reaction.

III. PLASMA CHARACTERISTICS, CONSUMPTION, AND GENERATION OF PFCs IN AN ICP ETCHING REACTOR

Schematics of the plasma etching chamber and burn-box used in this study are shown in Fig. 1. The plasma etching chamber is a 13.56 MHz ICP reactor with four coils on top of a dielectric window using Ar/C_2F_6 (or Ar/CF_4) as the process gas mixture at 10 mTorr. A 20 cm diameter silicon wafer with a conductivity of 0.05 $(\Omega\,cm)^{-1}$ sits on the substrate. The feedstock gas flows into the chamber through a showerhead nozzle and the exhaust gases are pumped out at the bottom of the chamber. The burn-box, which is located downstream of a turbopump, is also an ICP reactor operating at a higher pressure of 150 mTorr. O_2, H_2, or H_2O are injected into the burn-box as additive gases through a ring nozzle at the top of the reactor. The input fluxes to the burn-box are obtained from the output fluxes of the etching chamber. We assumed there were no compositional changes of the effluent in the turbopump. This is a simplifying assumption since there can be fluorocarbon films deposited inside the turbopump. The figure indicates a quartz tube for the burn-box which will likely be eroded and etched by the high fluorine content of the plasma. Actual systems use nonetching materials such as alumina,[7] and so we have not including wall etching reactions.

The baseline case for the plasma etching reactor uses an $Ar/C_2F_6=60/40$ mixture at 10 mTorr with 650 W ICP power. The power deposition, electron density, and the electron source for this case are shown in Fig. 2. The power deposition has a maximum of ≈ 1.7 W/cm^3 located off axis, 0.5 cm below the quartz window, and under the two middle coils. Since diffusion is the dominant mechanism for electron transport, the electron density (peak value of 2.2×10^{11} cm^{-3}) and the electron source have maximum values near the reactor axis. (No attempt was made to make reactive fluxes to the substrate uniform.) Positive ions (Ar^+ and CF_3^+) are first dominantly generated by electron impact ionization

TABLE II. Additional reaction and species for $Ar/CF_4/C_2F_6/O_2/H_2/H_2O$.[a] Species: O_2, O_2^+, O, O^*, O^+, O^-, H_2, H_2^+, H, H^-, H_2O, H_2O^+, OH, OH^-, H_3O^+, HO_2, HF, F^+, F_2^+, CF, $C_2F_4^+$, $C_2F_5^+$, CF_3O_2, COF_2, COF, CO, CO_2, FO, C.

Reaction	Rate coefficient[b]	Reference
$e+O_2 \rightarrow O^- + O$	c	36
$e+O_2 \rightarrow O(^1D)+O+e$	c	36
$e+O_2 \rightarrow O+O+e$	c	36
$e+O_2 \rightarrow O_2^+ +e+e$	c	36
$e+O_2 \rightarrow O^+ +O+e+e$	c	37
$e+O \rightarrow O(^1D)+e$	c	38
$e+O \rightarrow O^+ +e+e$	c	38
$e+O(^1D) \rightarrow O+e$	c	38
$e+O(^1D) \rightarrow O^+ +e+e$	c	38
$e+CF_2 \rightarrow CF+F+e$	c	24[d]
$e+CF_2 \rightarrow CF+F^-$	c	24[d]
$e+F_2 \rightarrow F^- +F$	c	39
$e+F_2 \rightarrow F+F+e$	c	39
$e+F_2 \rightarrow F_2^+ +e+e$	c	39
$e+F \rightarrow F^+ +e+e$	c	40
$e+CF_3O_2 \rightarrow CF_3+O_2+e$	c	24[d]
$e+C_2F_3 \rightarrow CF+CF_2+e$	c	25[e]
$e+COF_2 \rightarrow COF+F+e$	c	24[d]
$e+CO_2 \rightarrow CO+O+e$	c	41
$e+CO_2 \rightarrow CO+O^-$	c	41
$e+H_2 \rightarrow H+H+e$	c	42
$e+H_2 \rightarrow H_2^+ +e+e$	c	42
$e+H_2 \rightarrow H+H+e$	c	42
$e+H_2 \rightarrow H+H+e$	c	42
$e+H_2^+ \rightarrow H+H$	c	42
$e+H_2O \rightarrow OH+H^-$	c	43
$e+H_2O \rightarrow OH+H+e$	c	43
$e+H_2O \rightarrow O(^1D)+H_2+e$	c	43
$e+H_2O \rightarrow H_2O^+ +e+e$	c	43
$e+H_2O^+ \rightarrow O+H_2$	1.0×10^{-7}	44
$e+O_2^+ \rightarrow O(^1D)+O$	2.0×10^{-8}	45[d]
$e+F_2^+ \rightarrow F+F$	2.0×10^{-8}	45[d]
$Ar^+ +O_2 \rightarrow O_2^+ +Ar$	5.1×10^{-11}	46
$Ar^+ +O \rightarrow O^+ +Ar$	1.0×10^{-11}	47
$Ar^*+O_2 \rightarrow O+O+Ar$	2.1×10^{-10}	48
$Ar^*+O \rightarrow O(^1D)+Ar$	4.1×10^{-11}	49
$Ar^*+H_2 \rightarrow Ar+H+H$	2.1×10^{-10}	48
$Ar^*+H_2O \rightarrow Ar+OH+H$	2.1×10^{-10}	48
$Ar^+ +H_2 \rightarrow Ar+H_2^+$	1.0×10^{-9}	49
$Ar^+H_2O \rightarrow Ar+H_2O^+$	1.4×10^{-9}	49
$F^+ +H_2 \rightarrow H_2^+ +F$	1.2×10^{-9}	49
$F^+ +H_2O \rightarrow H_2O^+ +F$	7.97×10^{-11}	49
$F^- +H \rightarrow e+HF$	1.6×10^{-9}	49
$H^- +H \rightarrow e+H_2$	1.8×10^{-9}	49
$H^- +H_2O \rightarrow OH^- +H_2$	3.7×10^{-9}	49
$H^- +Ar^+ \rightarrow H+Ar$	1.0×10^{-7}	31[d]
$H^- +CF_3^+ \rightarrow H+CF_3$	1.0×10^{-7}	31[d]
$H^- +O_2^+ +M \rightarrow HO_2+M$	1.2×10^{-25} cm^6 s^{-1}	31[d]
$H^- +O^+ +M \rightarrow OH+M$	1.2×10^{-25} cm^6 s^{-1}	31[d]
$H^- +F^+ +M \rightarrow HF+M$	1.2×10^{-25} cm^6 s^{-1}	31[d]
$H^- +F_2^+ \rightarrow H+F_2$	5.0×10^{-8}	31[d]
$H^- +C_2F_4^+ \rightarrow H+C_2F_4$	1.0×10^{-7}	31[d]
$H^- +C_2F_5^+ \rightarrow H+C_2F_5$	1.0×10^{-7}	31[d]
$OH^- +H \rightarrow e+H_2O$	1.4×10^{-9}	49
$OH^- +O \rightarrow e+HO_2$	2.0×10^{-10}	49
$OH^{-1} +Ar^+ \rightarrow OH+Ar$	1.0×10^{-7}	31[d]
$OH^- +CF_3^+ \rightarrow OH+CF_3$	1.0×10^{-7}	31[d]
$OH^- +O_2^+ \rightarrow OH+O_2$	1.0×10^{-7}	31[d]
$OH^- +O^+ \rightarrow OH+O$	1.0×10^{-7}	31[d]
$OH^- +F^+ \rightarrow OH+F$	1.0×10^{-7}	31[d]
$OH^- +F_2^+ \rightarrow OH+F_2$	1.0×10^{-7}	31[d]
$OH^- +C_2F_4^+ \rightarrow OH+C_2F_4$	1.0×10^{-7}	31[d]
$OH^- +C_2F_5^+ \rightarrow OH+C_2F_5$	1.0×10^{-7}	31[d]
$H_2^+ +O_2 \rightarrow O_2^+ +H_2$	7.56×10^{-9}	49
$H_2^+ +C_2F_6 \rightarrow CF_3^+ +CF_3+H_2$	5.0×10^{-10}	49
$H_2^+ +H_2O \rightarrow H_2+H_2O^+$	3.6×10^{-9}	49
$H_2^+ +CF_3^- \rightarrow H_2+CF_3$	1.0×10^{-7}	31[d]
$H_2^+ +F^- \rightarrow H_2+F$	1.0×10^{-7}	31[d]
$H_2^+ +O^- \rightarrow H_2+O$	1.0×10^{-7}	31[d]
$H_2^+ +H^- \rightarrow H_2+H$	1.0×10^{-7}	31[d]
$H_2^+ +OH^- \rightarrow H_2+OH$	1.0×10^{-7}	31[d]
$H_2O^+ +CF_3^- \rightarrow H_2O+CF_3$	1.0×10^{-7}	31[d]
$H_2O^+ +F^- \rightarrow H_2O+F$	1.0×10^{-7}	31[d]
$H_2O^+ +O^- \rightarrow H_2O+O$	1.0×10^{-7}	31[d]
$H_2O^+ +H^- \rightarrow H_2O+H$	1.0×10^{-7}	31[d]
$H_2O^+ +OH^- \rightarrow H_2O+OH$	1.0×10^{-7}	31[d]
$H_2O^+ +H_2O \rightarrow H_3O^+ +OH$	1.7×10^{-9}	49
$H_3O^+ +e \rightarrow H_2O+H$	2.0×10^{-7}	44[d]
$H_3O^+ +H^- \rightarrow H_2+H_2O$	1.0×10^{-7}	31[d]
$H_3O^+ +O^- \rightarrow OH+H_2O$	1.0×10^{-7}	31[d]
$H_3O^+ +F^- \rightarrow H_2O+HF$	1.0×10^{-7}	31[d]
$H_3O^+ +CF_3^- \rightarrow H_2O+HF+CF_2$	1.0×10^{-7}	31[d]
$H_3O^+ +OH^- \rightarrow H_2O+H+OH$	1.0×10^{-7}	31[d]
$H+H+M \rightarrow H_2+M$	8.1×10^{-33} cm^6 s^{-1}	50
$H+OH+M \rightarrow H_2O+M$	$1.56\times10^{-31}(T/300)^{-1.21}$ exp$(295.3/T)$ cm^{-6} s^{-1}	51
$H+O+M \rightarrow OH+M$	4.33×10^{-32} cm^6 s^{-1}	52
$H+O_2+M \rightarrow HO_2+M$	$1.94\times10^{-32}(T/300)^{-0.7}$ exp$(144.3/T)$cm^6 s^{-1}	51
$H+HO_2 \rightarrow O+H_2O$	$3.84\times10^{-11}(T/300)^{-0.46}$ exp$(-677.9/T)$	52
$H+HO_2 \rightarrow H_2+O_2$	$2.34\times10^{-11}(T/300)^{-0.59}$ exp$(-320.8/T)$	52
$H+HO_2 \rightarrow OH+OH$	1.58×10^{-10} exp$(-365.2/T)$	52
$H+CF_3 \rightarrow CF_2+HF$	9.0×10^{-11}	53
$H+CF_2 \rightarrow CF+HF$	3.32×10^{-10} exp$(-629/T)$	34
$H+CF \rightarrow C+HF$	1.9×10^{-11}	34
$H+C_2F_5 \rightarrow C_2F_4+HF$	2.0×10^{-11}	34
$H+F_2 \rightarrow F+HF$	1.53×10^{-11}	34
$H+COF \rightarrow CO+HF$	1.93×10^{-10}	34
$C+O_2 \rightarrow CO+O$	3.3×10^{-11}	54
$H_2+F \rightarrow HF+H$	1.43×10^{-10} exp$(-528.0/T)$	34
$H_2+O(^1D) \rightarrow OH+H$	1.1×10^{-10}	55
$OH+F \rightarrow O+HF$	3.32×10^{-11}	34
$OH+CF_3 \rightarrow COF_2+HF$	3.32×10^{-11}	34
$OH+CF_2 \rightarrow COF+HF$	6.64×10^{-12} exp$(-1762.5/T)$	34
$OH+CF \rightarrow HF+CO$	6.64×10^{-11} exp$(-503/T)$	34
$OH+CO \rightarrow H+CO_2$	$1.18\times10^{-13}(T/300)^{-0.98}$ exp$(-94.3/T)$	34
$HO_2+F \rightarrow O_2+HF$	8.28×10^{-11}	56
$HO_2+CF_3 \rightarrow COF_2+HF+O$	1.66×10^{-11}	34
$HO_2+CF_2 \rightarrow COF_2+OH$	1.66×10^{-11} exp$(-1762.5/T)$	34
$HO_2+O \rightarrow OH+O_2$	3.0×10^{-11} exp$(200/T)$	57
$HO_2+OH \rightarrow H_2O+O_2$	5.1×10^{-11}	58
$H_2O+F \rightarrow OH+HF$	$1.11\times10^{-11}(T/300)^{1.5}$	34
$H_2O+O(^1D) \rightarrow OH+OH$	2.5×10^{-10}	59
$O^+ +CF_4 \rightarrow CF_3^+ +FO$	1.4×10^{-9}	60
$O^+ +CF_3 \rightarrow CF_3^+ +O$	1.0×10^{-10}	49
$O^+ +C_2F_6 \rightarrow CF_3^+ +CF_3+O$	1.47×10^{-9}	60
$O^+ +C_2F_6 \rightarrow C_2F_5^+ +FO$	3.0×10^{-11}	60
$O^+ +C_2F_4 \rightarrow C_2F_4^+ +O$	1.3×10^{-9}	29
$F^+ +CF_4 \rightarrow CF_3^+ +F_2$	1.0×10^{-9}	29
$F^+ +CF_3 \rightarrow CF_3^+ +F$	1.0×10^{-9}	29
$F^+ +C_2F_6 \rightarrow C_2F_5^+ +F_2$	1.0×10^{-9}	29
$F^+ +C_2F_5 \rightarrow C_2F_4^+ +F_2$	1.0×10^{-9}	29
$F^+ +C_2F_4 \rightarrow C_2F_4^+ +F$	1.0×10^{-9}	29

TABLE II. (*Continued*).

Reaction	Rate coefficient[b]	Reference	Reaction	Rate coefficient[b]	Reference
$F^{+}+O\rightarrow O^{+}+F$	1.0×10^{-10}	29	$O^{-}+O\rightarrow O_2+e$	3.0×10^{-10}	49
$F^{+}+O_2\rightarrow O_2^{+}+F$	6.4×10^{-10}	29	$O+O+M\rightarrow O_2+M$	1.0×10^{-33} cm^6 s^{-1}	50
$F^{+}+O_2\rightarrow O^{+}+FO$	1.6×10^{-10}	29	$O(^1D)+CF_4\rightarrow O+CF_4$	1.8×10^{-13}	33
$F^{+}+F\rightarrow F+F^{+}$	1.0×10^{-9}	29[d]	$O(^1D)+COF_2\rightarrow O+COF_2$	5.3×10^{-11}	33
$F_2^{+}+CF_4\rightarrow CF_3^{+}+F+F_2$	1.0×10^{-10}	29[d]	$O(^1D)+COF_2\rightarrow F_2+CO_2$	2.1×10^{-11}	33
$F_2^{+}+CF_3\rightarrow CF_3^{+}+F_2$	1.0×10^{-10}	29[d]	$O(^1D)+O_2\rightarrow O+O_2$	$3.2\times10^{-11}\exp(67/T)$	55
$F_2^{+}+C_2F_4\rightarrow C_2F_4^{+}+F_2$	1.0×10^{-10}	29[d]	$O(^1D)+CF_3\rightarrow COF_2+F$	3.1×10^{-11}	33
$F_2^{+}+C_2F_5\rightarrow C_2F_5^{+}+F_2$	1.0×10^{-10}	29[d]	$O(^1D)+CF_2\rightarrow COF+F$	1.4×10^{-11}	33
$F_2^{+}+F_2\rightarrow F_2^{+}+F_2$	1.0×10^{-9}	29[d]	$O(^1D)+CF_2\rightarrow CO+F+F$	4.0×10^{-12}	33
$O_2^{+}+C_2F_4\rightarrow C_2F_4^{+}+O_2$	9.8×10^{-10}	28	$O(^1D)+CF\rightarrow CO+F$	$6.64\times10^{-11}\exp(-503/T)$	33
$O_2^{+}+C_2F_5\rightarrow C_2F_5^{+}+O_2$	1.0×10^{-10}	28[d]	$O(^1D)+COF\rightarrow CO_2+F$	9.3×10^{-11}	33
$O_2^{+}+O_2\rightarrow O_2^{+}+O_2$	1.0×10^{-9}	29	$O(^1D)+CF_3O_2\rightarrow COF_2+F+O_2$	1.0×10^{-11}	33
$F^{-}+O_2^{+}\rightarrow F+O_2$	1.0×10^{-7}	31[d]	$O(^1D)+FO\rightarrow O_2+F$	5.0×10^{-11}	33
$F^{-}+O^{+}\rightarrow F+O$	1.0×10^{-7}	31[d]	$O+CF_3\rightarrow COF_2+F$	3.1×10^{-11}	33
$F^{-}+F_2^{+}\rightarrow F+F_2$	1.0×10^{-7}	31[d]	$O+CF_2\rightarrow COF+F$	1.4×10^{-11}	33
$F^{-}+F^{+}\rightarrow F+F$	1.0×10^{-7}	31[d]	$O+CF_2+\rightarrow CO+F+F$	4.0×10^{-12}	33
$F+CF_3\rightarrow CF_4$	$4.9\times10^{-9}(T/300)^{-7.84}$ $\exp(-1876.4/T)$	35	$O+CF\rightarrow CO+F$	6.64×10^{-11} $\exp(-503/T)$	34
$F+CF_2\rightarrow CF_3$	4.14×10^{-14}	33	$O+COF\rightarrow CO_2+F$	9.3×10^{-11}	33
$F+COF\rightarrow COF_2$	2.76×10^{-13}	33	$O+CF_3O_2\rightarrow COF_2+F+O_2$	1.0×10^{-11}	33
$F+CO\rightarrow COF$	3.87×10^{-16}	33	$O+FO\rightarrow O_2+F$	5.0×10^{-11}	33
$O^{-}+Ar^{+}O+Ar$	1.0×10^{-7}	31[d]	$O+F+M\rightarrow FO+M$	1.0×10^{-33} cm^6 s^{-1}	34
$O^{-}+O_2^{+}\rightarrow O+O_2$	1.0×10^{-7}	31[d]	$O+C_2F_5\rightarrow COF_2+CF_3$	3.65×10^{-11}	34
$O^{-}+O^{+}\rightarrow O+O$	1.0×10^{-7}	31[d]	$O_2+CF_3\rightarrow CF_3O_2$	4.44×10^{-14}	34
$O^{-}+F_2^{+}\rightarrow O+F_2$	1.0×10^{-7}	31[d]	$COF+CF_2\rightarrow CF_3+CO$	3.0×10^{-13}	34
$O^{-}+F^{+}\rightarrow O+O$	1.0×10^{-7}	31[d]	$COF+CF_2\rightarrow COF_2+CF$	3.0×10^{-13}	34
$O^{-}+CF_3^{+}\rightarrow O+CF_3$	1.0×10^{-7}	31[d]	$COF+CF_3\rightarrow CF_4+CO$	1.0×10^{-11}	34
$O^{-}+C_2F_4^{+}\rightarrow O+C_2F_4$	1.0×10^{-7}	31[d]	$COF+CF_3\rightarrow COF_2+CF_2$	1.0×10^{-11}	34
$O^{-}+C_2F_5^{+}\rightarrow O+C_2F_5$	1.0×10^{-7}	31[d]	$COF+COF\rightarrow COF_2+CO$	1.0×10^{-11}	34
$CF_3^{-}+O_2^{+}\rightarrow CF_3+O_2$	1.0×10^{-7}	31[d]	$COF+OH\rightarrow CO_2+CO_2$	1.0×10^{-11}	34
$CF_3^{-}+O^{+}\rightarrow CF_3+O$	1.0×10^{-7}	31[d]	$CF_2+CF_3\rightarrow C_2F_5$	5.36×10^{-12}	34
$CF_3^{-}+F_2^{+}\rightarrow CF_3+F_2$	1.0×10^{-7}	31[d]	$CF_3+CF_3\rightarrow C_2F_6$	7.26×10^{-12}	34
$CF_3^{-}+F^{+}\rightarrow CF_3+CF_3$	1.0×10^{-7}	31[d]			

[a]Only reactions directly affecting species densities are shown here. Additional electron impact collisions (e.g., momentum transfer, vibrational excitation) are included in the EETM.
[b]Rate coefficients have units cm^3 s^{-1} unless noted otherwise.
[c]Computed using the electron energy distribution and electron impact cross section from cited reference.
[d]Estimated. See cited reference for similar reaction.

of Ar*, Ar, and C_2F_6, and secondarily by dissociative charge transfer of Ar^+ to C_2F_6 and its fragments. Negative ions (F^- and CF_3^-) are generated by electron impact dissociative attachment, first of the feedstock C_2F_6 and secondarily from the dissociation fragments. Ion densities, shown in Fig. 3, have the same general shape as the electron density with the exception that the dominant negative ion, F^-, is less extended due to its trapping at the peak of the plasma potential. Since there is charge exchange to C_2F_6 and Ar has the higher ionization threshold (16 eV for Ar and 14.2 eV C_2F_6), the peak density of Ar^+(1.96×10^{11} cm^{-3}) is about 0.7 times that of CF_3^+ (2.75×10^{11} cm^{-3}) even though there is a larger Ar input gas mole fraction. The negative ions are dominated by F^- with an on-axis maximum density of 2.24×10^{11} cm^{-3} (about 0.9 times the electron density) which is two orders of magnitude larger than that of CF_3^-. F^- generation by electron impact dissociative attachment occurs by at least fourdissociative attachment processes and by charge transfer from CF_3^-,

$$e+C_2F_6\rightarrow C_2F_5+F^-, \quad (8a)$$

$$e+C_2F_5\rightarrow C_2F_4+F^-, \quad (8b)$$

$$e+CF_3\rightarrow CF_2+F^-, \quad (8c)$$

$$e+CF_2\rightarrow CF+F^-, \quad (8d)$$

$$CF_3^-+F\rightarrow CF_3+F^-. \quad (8e)$$

CF_3^- is dominantly generated only by electron impact dissociative attachment from C_2F_6 and CF_4.

The densities of C_2F_6, CF_3, and CF_2 are shown in Fig. 4. The C_2F_6 is quickly dissociated upon injection into the plasma. There is some reformation of C_2F_6 in the plasma and on walls. CF_3 is a primary fragment of dissociative electronic excitation of C_2F_6 and dissociative excitation transfer from Ar* to C_2F_6, while CF_2 is produced by dissociation of CF_3 and CF_4. Due to subsequent reassociation, the density of CF_3

TABLE III. Reactive sticking coefficients for species on walls and wafer.

Species	Boundary	Reaction probability	Species returning to plasma
Ar	walls or wafer	1.0	Ar
Ar^+	walls or wafer	1.0	Ar
Ar*	walls or wafer	1.0	Ar
CF_4	walls or wafer	1.0	CF_4
CF_3	walls or wafer	0.995	CF_3
	walls or wafer	0.005	0.5 C_2F_6
CF_3^+	walls or wafer	1.0	CF_3
CF_3^-	walls or wafer	1.0	CF_3
CF_2	walls	0.990	CF_2
	walls	0.010	0.5 C_2F_4
	wafer	0.940	CF_2
	wafer	0.060	0.5 (C_2F_3+SiF_2)
F	walls	0.995	F
	walls	0.005	0.5 F_2
	wafer	0.900	F
	wafer	0.100	0.5 SiF_2
F^-	walls or wafer	1.0	F
F_2	walls or wafer	1.0	F_2
C_2F_3	walls or wafer	1.0	C_2F_3
C_2F_4	walls or wafer	1.0	C_2F_4
C_2F_5	walls or wafer	1.0	C_2F_5
C_2F_6	walls or wafer	1.0	C_2F_6
SiF_2	walls or wafer	1.0	SiF_2

increases near the pump port, while the density of CF_2 has a maximum at the reactor axis due to its continuous loss (recombination of CF_2 with F, F_2, CF_3, and itself) after being produced. Other C_xF_y species (C_2F_4, C_2F_5, and CF_4), shown in Fig. 5, are slowly generated by radical recombination through gas phase and wall reactions. The mole fractions of neutral species in the effluent from our baseline etching reactor consist of

Ar	0.415	CF_3	0.141	CF_2	0.111
C_2F_6	0.093	SiF_2	0.074	F	0.071
CF_4	0.047	C_2F_3	0.018	C_2F_5	0.018
F_2	0.009	C_2F_4	0.003		

The total output flow rate is 242.8 sccm, larger than the input flow rate due to dissociation.

Since CF_4 is frequently used as a process gas, we also examined Ar/CF_4 ICP etching discharges. The baseline case is the same as that for Ar/C_2F_6 with the exception that CF_4 replaces C_2F_6. The shapes of the profiles of electron, ions, and neutrals do not appreciably change. The mole fractions in the effluent for the Ar/CF_4 base case are

Ar	0.477	CF_3	0.066	CF_2	0.077
C_2F_6	0.008	SiF_2	0.090	F	0.117
CF_4	0.132	C_2F_3	0.012	C_2F_5	0.004
F_2	0.014	C_2F_4	0.002		

The total output flowrate of 212.7 sccm is smaller than that for the Ar/C_2F_6 case corresponding to a lower total amount of dissociation.

A design of experiments (DOE) was performed to char-

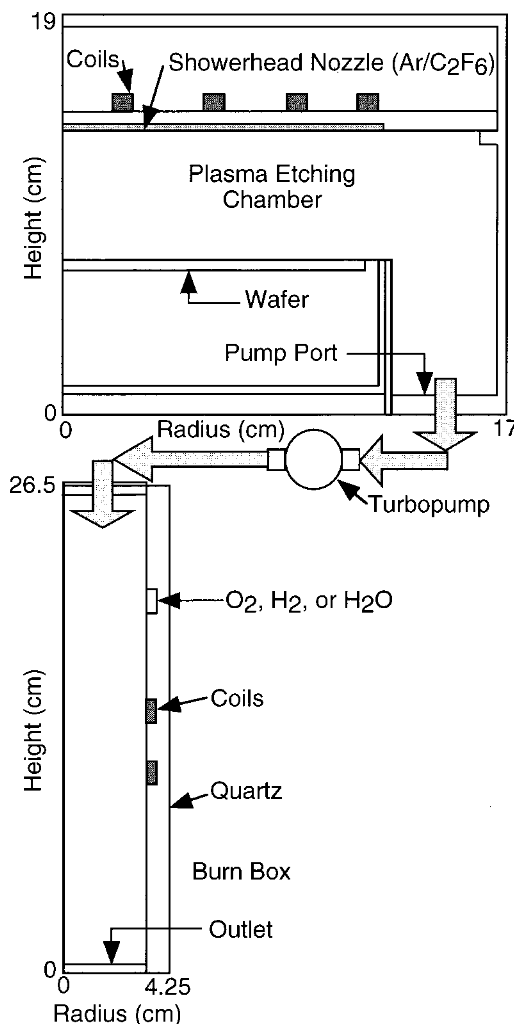

FIG. 1. Schematics of the inductively coupled plasma etching reactor and plasma burn-box. The coils for both of the devices are driven at 13.56 MHz. A turbopump is between the etching reactor and burn-box.

acterize the consumption of C_2F_6 in the etching chamber. The fractional consumption of C_2F_6 in the etching chamber as a function of mole fraction of C_2F_6 (20%–60%), gas flow rate (100–300 sccm), and power deposition (350–650 W) is shown in Fig. 6. The consumption is based on the outflow (sccm) compared to the inflow (sccm). The consumption scales almost linearly with power deposition, and decreases with increasing gas flow rate (shorter gas residence time) and input C_2F_6 mole fraction. Using higher power and lower flow rate, one expects to increase the C_2F_6 consumption since more energy is deposited per input C_2F_6 molecule. These results can be summarized in terms of energy per molecule (eV/molecule) required for consumption of C_2F_6. The energy, typically called the *W* value, is shown in Fig. 7. A small *W* value corresponds to higher efficiency. Low *W* values were obtained at high C_2F_6 mole fraction and high flow rate. At higher C_2F_6 mole fractions, there is a more power deposition into C_2F_6 relative to Ar, and for a higher flow rate, these is a less power expended in the dissociation products. The total generation of radicals (CF_2, CF_3, C_2F_3, C_2F_5,

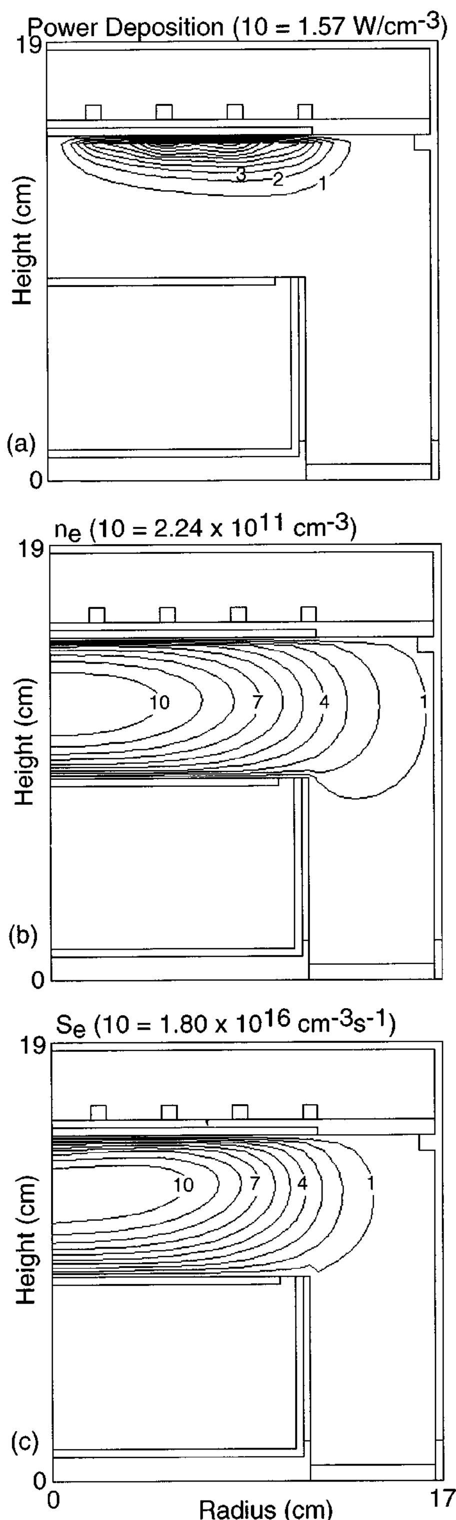

FIG. 2. Plasma parameters for the standard case for the plasma etching reactor (Ar/C_2F_6=60/40, 10 mTorr, and 650 W inductively coupled power). (a) Power deposition. (b) Electron density. (c) Electron source by electron impact. The contours are labeled by their relative magnitudes with the maximum values noted at the top of each figure.

and F) and other PFCs is almost linearly proportional to the C_2F_6 consumption.

A similar DOE was carried out for Ar/CF_4 gas mixtures. CF_4 shows similar systematic trends in consumption and in *W* values. However, for given conditions, the consumption is generally lower and *W* values higher than Ar/C_2F_6 due to the lower rate of dissociation of CF_4. Comparing the base line cases using Ar/C_2F_6 or Ar/CF_4=60/40 at 650 W, the consumption and *W* values are 72% and 158 eV molecule for C_2F_6, and 65% and 175 eV molecule for CF_4. The total generation of C_xF_y in the effluent for the CF_4 cases is approximately half that of the corresponding C_2F_6 cases. The output amounts of CF_2 and CF_3 for the C_2F_6 case are larger by factors of 2.44 and 1.65, respectively, compared to the CF_4 case, largely a consequence of the branching ratios for fragmentation of the feedstocks which favor CF_x production from C_2F_6. There are, however, slightly more F radicals in the effluent for Ar/CF_4 mixtures.

IV. PLASMA ABATEMENT OF PFCs IN THE BURN-BOX

In order to abate the PFCs emitted by the etching chamber, the effluent is passed through the plasma burn-box. The effluents for Ar/C_2F_6 discharges consist mainly of Ar, undissociated C_2F_6,CF_x radicals, newly generated PFCs (CF_4, C_2F_4, and C_2F_5), fluorine (F and F_2), and the etch product (SiF_2). In this section, we first present a comparison of our results with experiments for abatement of C_2F_6 for validation purposes, and then discuss the remediation of simulated effluent using O_2, H_2, or H_2O as additives.

A. Validation

The model was validated by comparing our results to experiments by Sawin and Vitale[9] for abatement of C_2F_6 in an ICP reactor. Their reactor is a 10 cm diameter stainless-steel tube with an internal coil. The feedstock gas was C_2F_6/O_2 =50/50. They found that C_2F_6 is decomposed in the plasma reactor, but CF_4 is generated as a product, which coincides with the observations of Hartz *et al.*[8]

The formation of CF_4 largely depends on the availability of F atoms to recombine with CF_3. Through our parametric studies we found that the branching ratio for $e+C_2F_6 \rightarrow C_2F_5+F^-$ or $CF_3+CF_3^-$ significantly impacts the net destruction of C_2F_6 and the formation of CF_4 for Sawin and Vitale's conditions. The branching ratios for electron impact dissociation products of fluorocarbons, particularly for dissociative attachment, are functions of the vibrational state and gas temperatures[61] and so there is some uncertainty in their values here. For example, the mole fractions of C_2F_6 remaining and CF_4 formation in the exhaust of the burn-box are shown in Fig. 8(a) as a function of the branching ratio of $e+C_2F_6 \rightarrow CF_3+CF_3^-$. The total flow rate is 400 sccm, the pressure is 500 mTorr, and the power deposition is 500 W. An increase in this branching (and decrease in branching for $C_2F_5+F^-$) produces more CF_3 which can recombine more rapidly with F to form CF_4 or with another CF_3 radical to reform C_2F_6. Any C_2F_5 generated can rapidly react with F to generate additional CF_3. A branching ratio of 58% best matches experimental data. Using this branching, comparisons between experiments and simulations as a function of

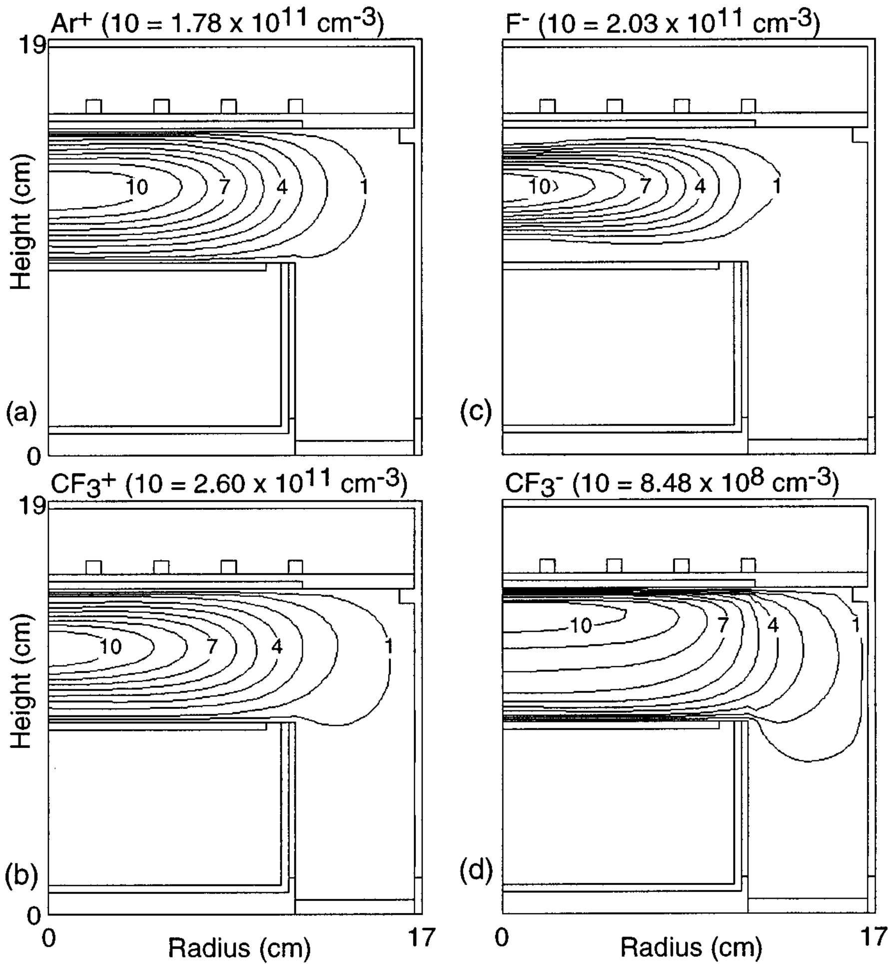

FIG. 3. Ion densities for the standard case for the plasma etching reactor. (a) Ar^+, (b) CF_3^+, (c) F^-, and (d) CF_3^-. The peak density of CF_3^+ is larger than that of Ar^+ though there is a larger Ar input mole fraction. The negative ions are dominated by F^-. The contours are labeled by their relative magnitudes with the maximum values noted at the top of each figure.

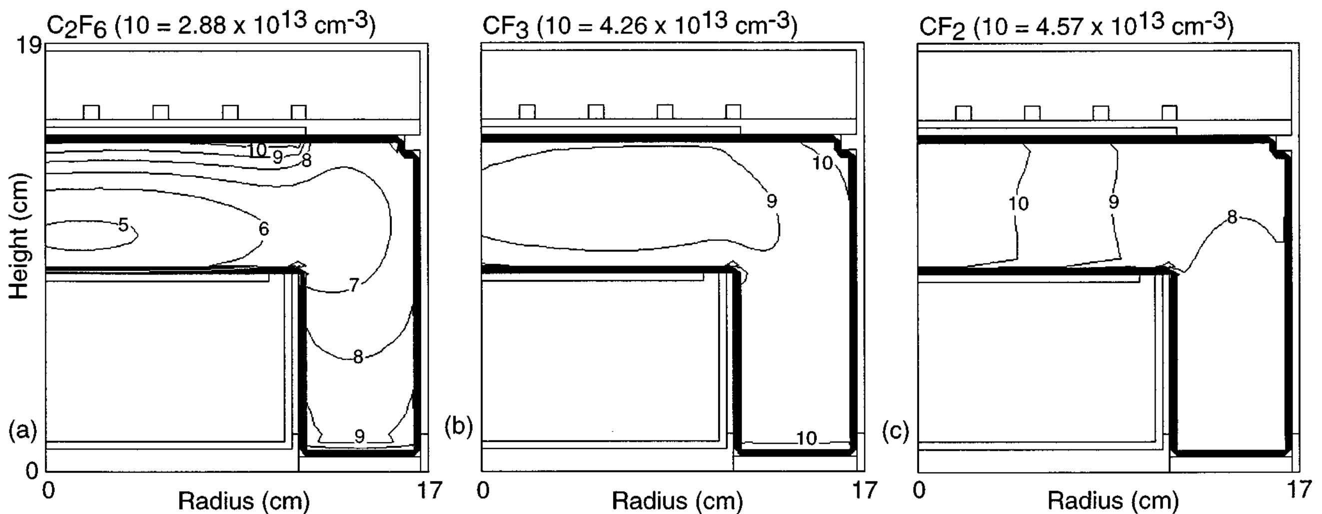

FIG. 4. Densities of input PFC and primary CF_x fragment densities for the standard case for the plasma etching reactor. (a) C_2F_6, (b) CF_3, and (c) CF_2. C_2F_6 is quickly dissociated upon injection into plasma. The density of CF_3 increases near surfaces due to recombination of plentiful CF_3^+. The contours are labeled by their relative magnitudes with the maximum values noted at the top of each figure.

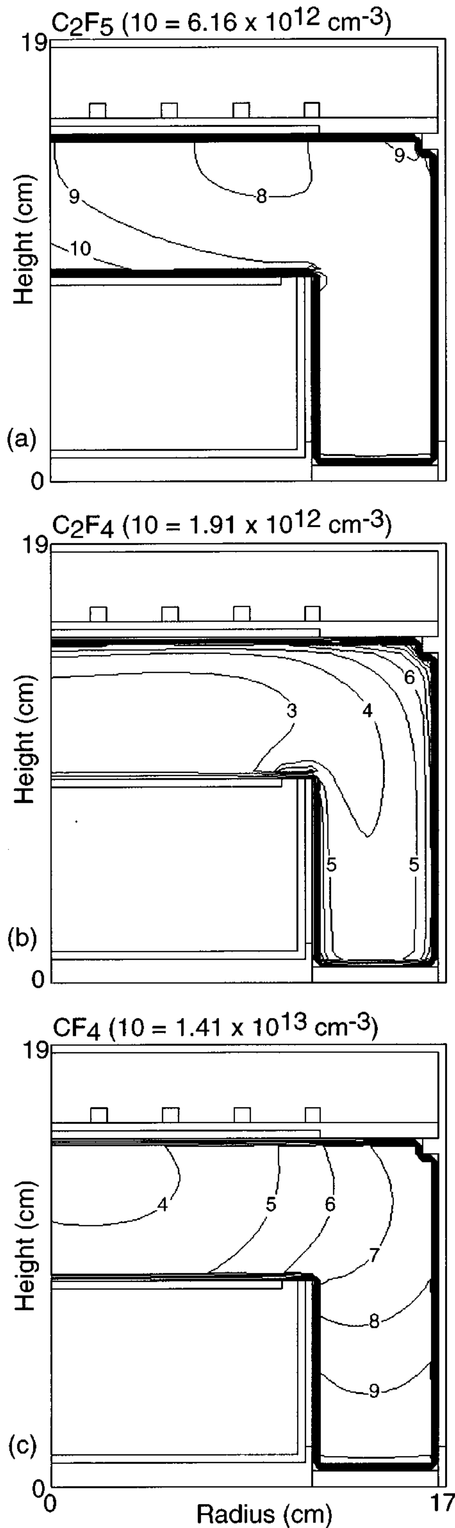

FIG. 5. Densities of PFCs generated by the process for the standard case of a plasma etching reactor. (a) C_2F_5, (b) C_2F_4, and (c) CF_4. These species are generated by radical recombination through gas phase and wall reactions.

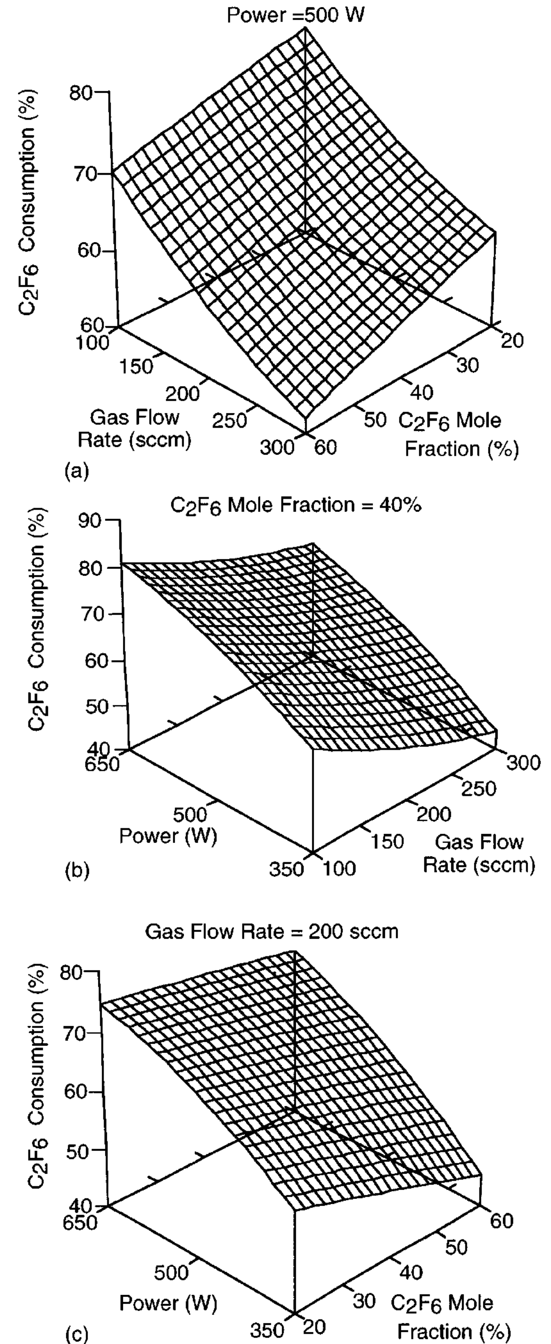

FIG. 6. Consumption of C_2F_6 in the plasma etching reactor as a function of power, gas flow rate, and input C_2F_6 mole fraction. (These figures are the results of a design of experiments whose response surface was fitted with a quadratic with cross terms. Some curvature of the surface results from the numerical fitting. Note that the independent variables have different orientations to obtain a better view angle.) The conditions held constant are: (a) Power at 500 W, (b) C_2F_6 mole fraction at 40%, and (c) gas flow rate at 200 sccm. Consumption of C_2F_6 increases with increasing power, decreasing flow rate, and decreasing C_2F_6 mole fraction.

power deposition are shown in Fig. 8(b). Over the range of power investigated, the model agrees well with the experiments. The C_2F_6 destruction increases with increasing power while the CF_4 production increases. At the highest power (1000 W) there is 40% C_2F_6 decomposition and 25% CF_4 generation.

At 500 mTorr, the plasma is generated dominantly near the coils due to the finite electromagnetic skin depth and rapid electron thermalization. (The electron thermalization

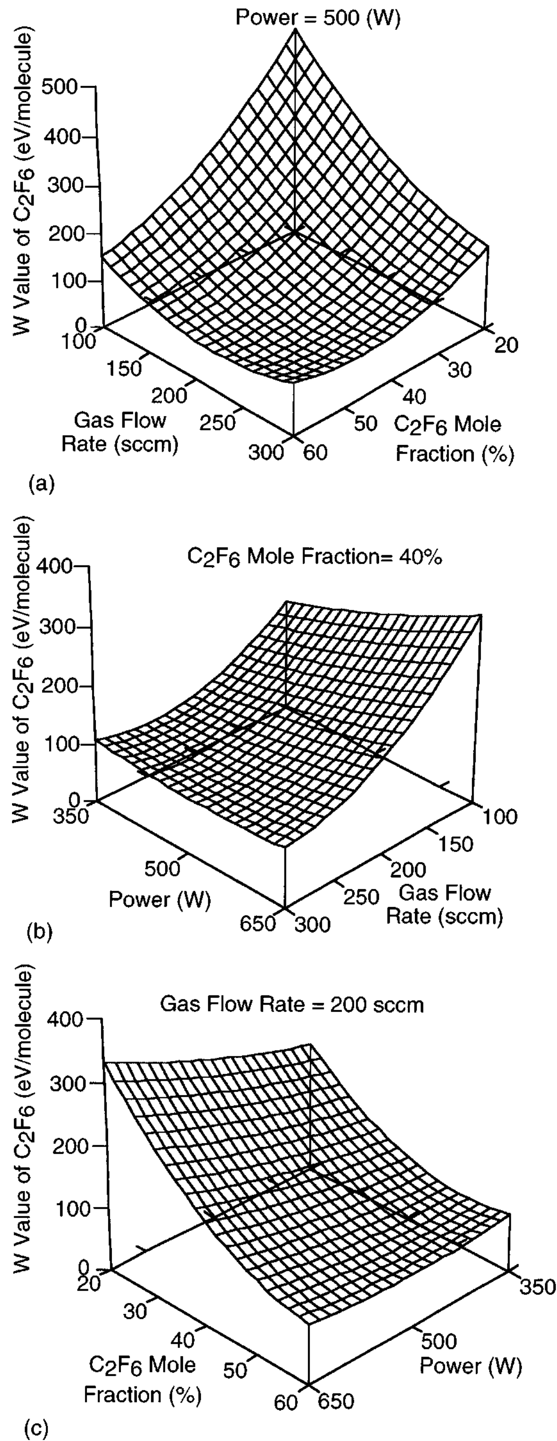

FIG. 7. W-values (eV/molecule) for consumption of C_2F_6 for the plasma etching reactor as a function of power, gas flow rate, and C_2F_6 mole fraction. The conditions held constant are: (a) Power at 500 W, (b) C_2F_6 input mole fraction of 40%, and (c) gas flow rate 200 sccm. Low W-values (high efficiency) are obtained at high C_2F_6 mole fraction and high flowrates. There is a weak dependence on power, with lower power being more efficient.

time at 2.6 eV, the peak electron temperature here, in an $C_2F_6/O_2=50/50$ mixture at 500 mTorr is ≈35 ns. In comparison, the thermalization time for an $Ar/C_2F_6=50/50$ mixture at 10 mTorr and 4 eV, typical of the plasma etching reactor, is 580 ns.) For example, the electron density, the rate

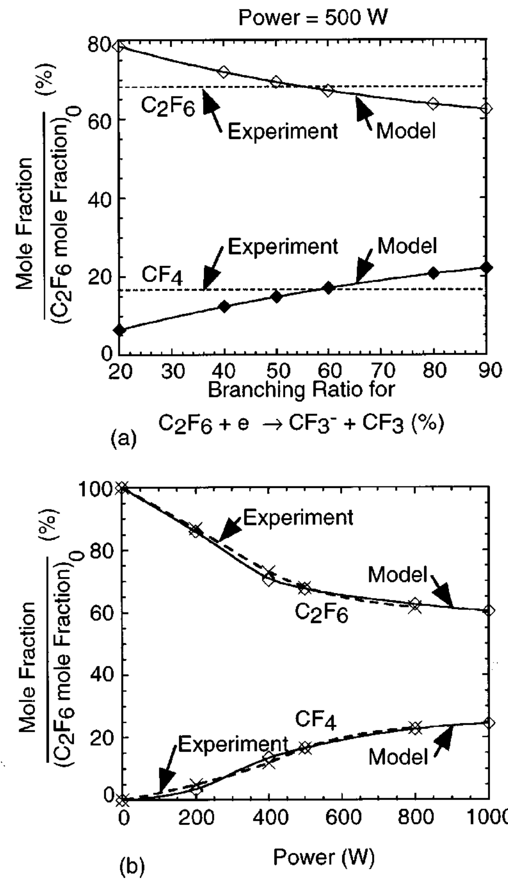

FIG. 8. Comparison of the mole fractions of C_2F_6 remaining and the formation of CF_4 obtained from the model and the experiments of Sawin and Vitale for a burn-box with an internal coil ($C_2F_6/O_2=50/50$, 500 mTorr, 400 sccm flow rate). (a) Mole fractions as a function of the branching ratio of $e+C_2F_6\rightarrow CF_3^-+CF_3$ at a power deposition of 500 W. (b) Mole fractions as a function of power with a branching ratio of 58%.

of electron impact dissociation of C_2F_6 and the advective gas velocity field for the 500 W case are shown in Fig. 9. The maximum electron density ($5.3\times10^{11}\,cm^{-3}$) is near the middle coil and decreases by a factor of 30 at the center of burn-box. The dissociation rate of C_2F_6 is correspondingly smaller in the center where the advective gas velocity is highest. This pass through of gases in the center of reactor contributes to the lower level of C_2F_6 degradation under the experimental conditions.[10]

As discussed later, CF_4 generation is by radical recombination between F and CF_3. At 500 mTorr, the rate constant of $CF_3+F\rightarrow CF_4$ for a gas temperature range of 300–1000 K is given by[35]

$$k_9=3.5\times10^{-8}\left(\frac{T_g}{298}\right)^{-7.73}\exp\left(-\frac{2210}{T_g}\right)\mathrm{cm^3/s}. \quad (9)$$

At 500 W, the mean gas temperature in the reactor is ≈400 K, at which $k_9=1.1\times10^{-11}\,cm^3/s$. As a result CF_4 production is favored. Higher mean gas temperatures can therefore result in lower rates of CF_4 production.

To quantify the destruction efficiency of all C_xF_y species, we define its W-value as the input power divided by the sum

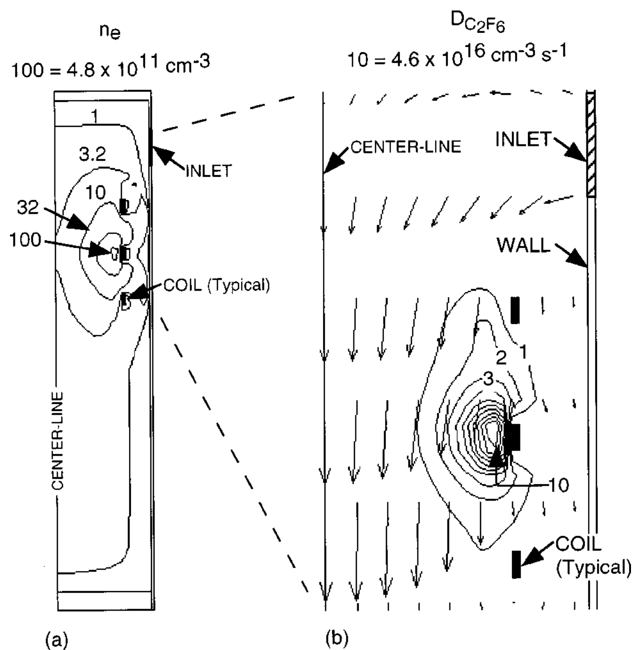

FIG. 9. Computed plasma parameters for the 500 W experimental case. (a) Electron density (with a logarithm scale). (b) Rate of electron impact dissociation of C_2F_6 with the advective field shown with vectors. The low abatement obtained with this case is partly a consequence of a large proportion of the C_2F_6 flowing through low plasma density regions.

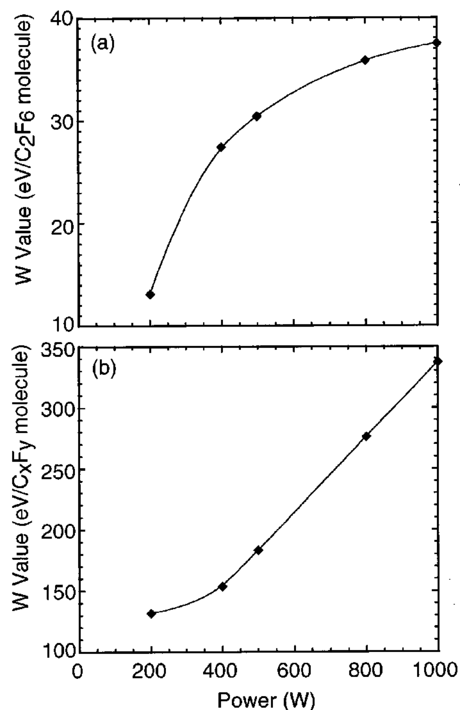

FIG. 10. W-values as a function of power for the experimental conditions. (a) W-values for C_2F_6 destruction. (b) W-values for destruction of all C_xF_y. The W-value of C_xF_y is higher than that of C_2F_6 since dissociation products of C_2F_6 form other C_xF_y species (as opposed to being oxidized).

of C_xF_y destruction weighted by the number of F atoms and normalized by 6 (the number of F atoms in C_2F_6),

$$W(C_xF_y)=\frac{P}{\Sigma_i[f_i(C_xF_y)y/6]_{\mathrm{input}}-\Sigma_i[f_i(C_xF_y)y/6]_{\mathrm{output}}}, \quad (10)$$

where P is the power deposition, f_i is the flow rate (input or output) of the ith C_xF_y. The W-value for C_xF_y would be equal to that for C_2F_6 if the compound was completely oxidized with there being no C_xF_y fragments. The weighting of the W-value with the number of F atoms in the molecule is a qualitative judgement that larger dissociation products are ''less good.'' W-values for C_2F_6 and for all C_xF_y as a function of power for the experimental conditions are shown in Fig. 10. $W(C_xF_y)$ is five to ten times larger than $W(C_2F_6)$ since more energy is required to abate the products of the dissociation of C_2F_6 than to simply destroy C_2F_6. Both W-values increase with increasing power indicating lower efficiency. Although higher power deposition produces higher densities of radicals, the higher radical densities result in more rapid rates of radical-radical recombination. As the power deposition increases and more dissociation is produced, the incremental dissociation is less efficient because more power goes into the dissociation products.

B. O_2 as an additive for PFC abatement

We first consider O_2 as an additive gas for abatement, in the plasma burn-box, of effluent from the etching chamber. The desired reaction pathway is to oxidize the carbon in C_xF_y to CO_2. Electron impact of O_2 generates O,O(^1D) and O^+, which in turn react with the PFCs and CF_x radicals mainly as follows:

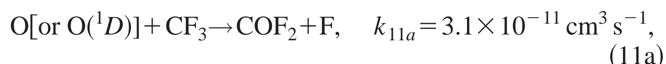

$$\mathrm{O[or\ O(^1D)]+CF_3\rightarrow COF_2+F}, \quad k_{11a}=3.1\times10^{-11}\ \mathrm{cm^3\,s^{-1}}, \quad (11a)$$

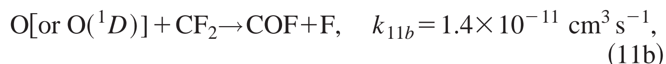

$$\mathrm{O[or\ O(^1D)]+CF_2\rightarrow COF+F}, \quad k_{11b}=1.4\times10^{-11}\ \mathrm{cm^3\,s^{-1}}, \quad (11b)$$

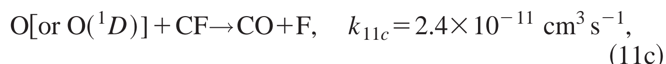

$$\mathrm{O[or\ O(^1D)]+CF\rightarrow CO+F}, \quad k_{11c}=2.4\times10^{-11}\ \mathrm{cm^3\,s^{-1}}, \quad (11c)$$

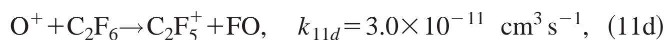

$$\mathrm{O^++C_2F_6\rightarrow C_2F_5^++FO}, \quad k_{11d}=3.0\times10^{-11}\ \mathrm{cm^3\,s^{-1}}, \quad (11d)$$

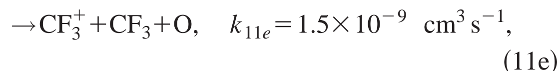

$$\mathrm{\rightarrow CF_3^++CF_3+O}, \quad k_{11e}=1.5\times10^{-9}\ \mathrm{cm^3\,s^{-1}}, \quad (11e)$$

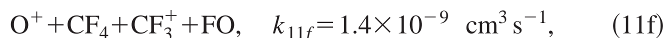

$$\mathrm{O^++CF_4+CF_3^++FO}, \quad k_{11f}=1.4\times10^{-9}\ \mathrm{cm^3\,s^{-1}}, \quad (11f)$$

where rate coefficients are shown for $T_g=500$ K. The dominant reaction products of O atoms with CF_x are COF, COF_2, and CO. It is important to note that at low gas temperatures O and O(^1D) do not directly react with CF_4 or C_2F_6, and O_2 is generally unreactive with C_xF_y fragments. Remediation dominantly occurs by radical-radical reactions. The desired end product CO_2 can be formed by reactions of COF with O or O(^1D), and COF_2 with O(^1D).

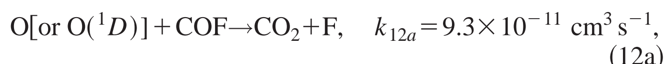

$$\mathrm{O[or\ O(^1D)]+COF\rightarrow CO_2+F}, \quad k_{12a}=9.3\times10^{-11}\ \mathrm{cm^3\,s^{-1}}, \quad (12a)$$

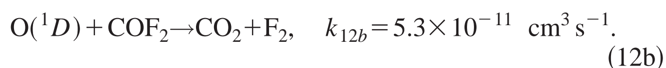

$$\mathrm{O(^1D)+COF_2\rightarrow CO_2+F_2}, \quad k_{12b}=5.3\times10^{-11}\ \mathrm{cm^3\,s^{-1}}. \quad (12b)$$

Although PFC dissociation primarily takes place through electron impact, there are several other pathways for dissociation (e.g., dissociative charge transfer with O^+, Ar^+, F^+, and F_2^+). For example, approximately 62% of CF_3 production is by direct electron impact of C_2F_6 and 10% results from charge transfer reactions.

The effluent comes into the burn-box through the top of the reactor, while O_2 is injected through a ring nozzle pointing radially inward. The plasma burn-box is cylindrical with an inner radius of 2.5 cm and a length of 26.5 cm. Two coils are placed near the middle of the tube with a power deposition of 500 W. The effluent from the plasma etching reactor operating at $Ar/C_2F_6=40/60$, 200 sccm flow rate and 350 W power is used as input for our base case. This case was selected because its effluent contains a relatively high mole fraction of C_2F_6(0.289) and there is a variety of other C_xF_y species (0.173 CF_3, 0.057 CF_4, 0.055 CF_2, 0.011 C_2F_4, and 0.02 C_2F_5). 150 sccm O_2 is injected as the additive. The power deposition, electron density, electron temperature, and plasma potential for this case are shown in Fig. 11. The peak electron density is $\approx 1.2\times 10^{12}\,cm^{-3}$ with an off-axis maximum located 7.3 mm from the side wall. The inductively coupled power deposition has a maximum of 15 W/cm^3 and is located approximately 3.3 mm inside the quartz tube. These peak values are larger than the plasma etching chamber due to the higher power density (W/cm^3) and the shorter electron energy relaxation length at the higher pressure. The distance of the peak power deposition from the wall is smaller than that in the plasma etching reactor due to the shorter skin depth resulting from a higher electron density. The electron temperature, peak value 3.1 eV, varies moderately near the coils in the radial direction and extends as a "hot zone" about 5 cm above and below the coils.

As the gas passes near the coils, the O_2 density rapidly decreases due to electron impact dissociation and ionization while the O density increases, as shown in Fig. 12. Dissociation of C_2F_6 in the plasma zone is dominated by electron impact processes as opposed to excitation transfer from Ar*. For example, the relative contributions to disassociation of (electron impact excitation): attachment: ionization: (excitation transfer from Ar*) are 23:18:13:1. Excitation transfer from Ar* to C_xF_y and O_2 does, however, dominate over energy pooling (e.g., Ar*+Ar*) by factor of 40 as a means for quenching Ar*. For our baseline case, CF_2, CF_3, C_2F_3, C_2F_4, and C_2F_5 are nearly totally eliminated (~100%), and C_2F_6 is decreased by 53% in passing through the burn-box. As shown in Figs. 12 and 13, their concentrations significantly decrease as the gas flow passes through the region near the coils where the oxygen radicals and electron densities are large. [O(^1D) and O^+ only have high densities in plasma region since they react with other species or quench quickly after being generated.] The concentrations of major oxidation products (CO,CO_2,COF_2) increase downstream of the coil region as does CF_4, as shown in Fig. 14. A summary of the abatement efficiencies and end products for the base case appears in Table IV.

Note that a significant amount of CF_4 is produced above

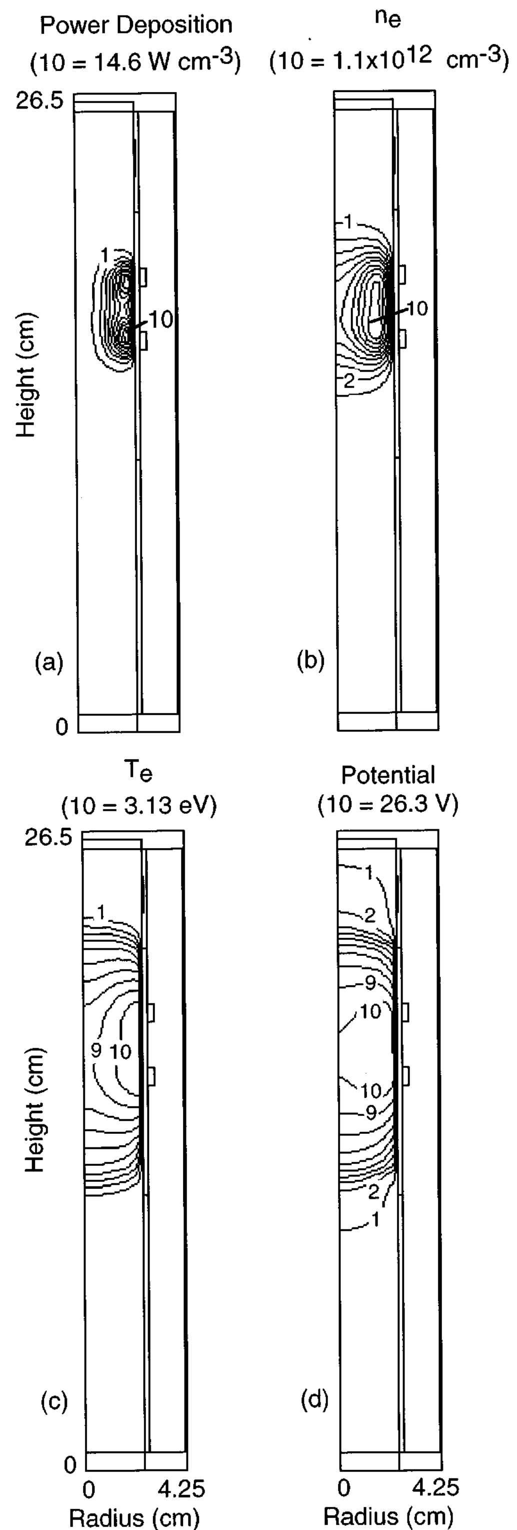

FIG. 11. Plasma parameters for the baseline case of a plasma burn-box using O_2 as an abatement additive gas. The base-case conditions are using effluent from the plasma etching chamber operating at $Ar/C_2F_6=40/60$, 10 mTorr, 200 sccm, 350 W, and the burn-box operating at 150 mTorr, 500 W with 150 sccm of injected O_2. (a) Power deposition, (b) electron density, (c) electron temperature, (d) plasma potential. The effluent comes in the burn-box through the top of the reactor and O_2 is injected through a ring nozzle pointing radially inward. The contours are labeled by their relative magnitudes with the maximum values noted at the top of each figure.

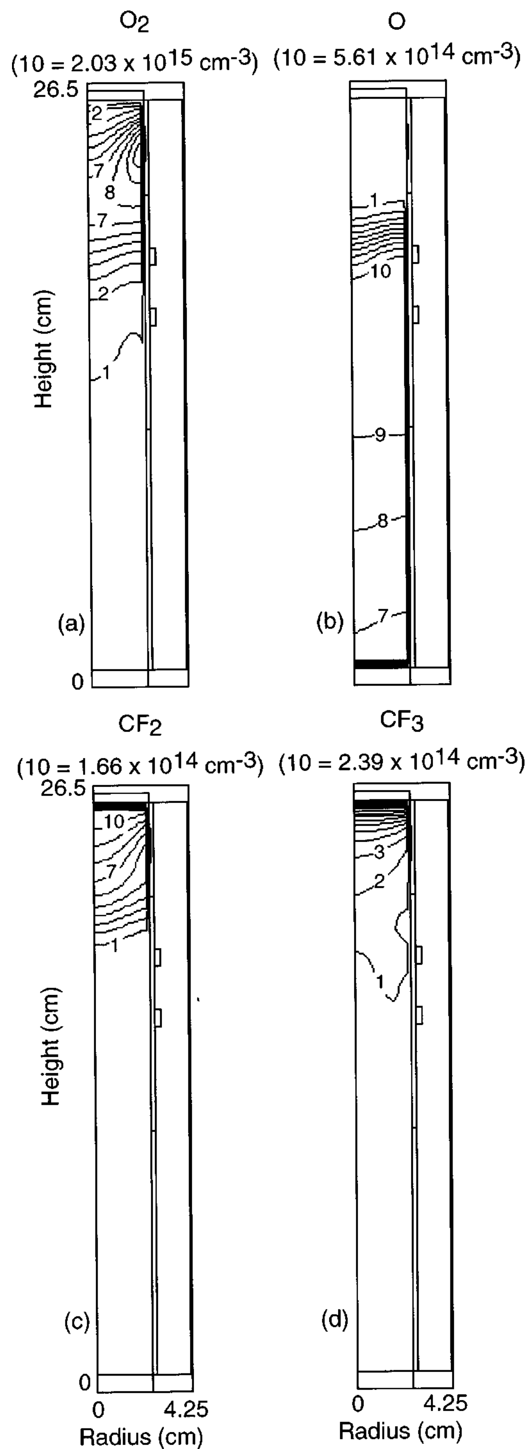

FIG. 12. Species densities for the baseline case of the plasma burn-box using O_2 as an additive. (a) O_2, (b) O, (c) CF_2, and (d) CF_3. O_2 is largely consumed in the plasma zone generating O radicals. CF_n is largely oxidized as it passes through the plasma zone. The contours are labeled by their relative magnitudes with the maximum values noted at the top of each figure.

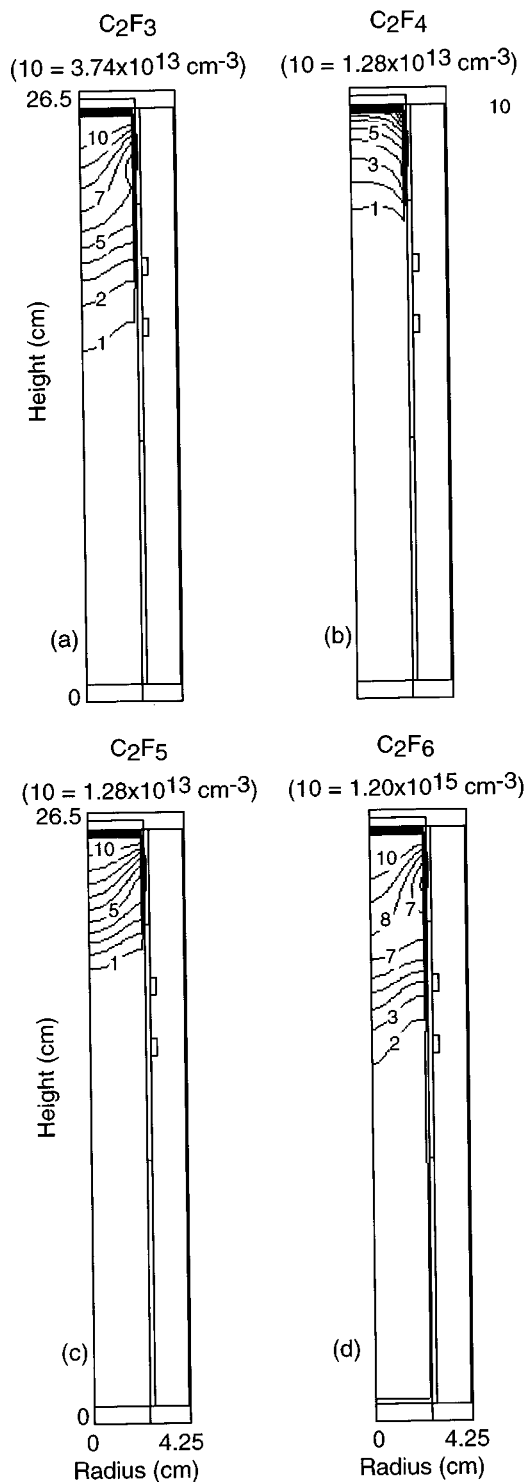

FIG. 13. Species densities for the baseline case of the plasma burn-box using O_2 as an additive. (a) C_2F_3, (b) C_2F_4, (c) C_2F_5, and (d) C_2F_6. Injected PFCs are largely abated by electron impact dissociation followed by oxidation. The contours are labeled by their relative magnitudes with the maximum values noted at the top of each figure.

the inlet value due to back diffusion of F atoms produced lower in the reactor which recombine with CF_3. The total amount of CF_4 in the gas stream actually increases by a factor of 2.4 for the base case. CF_4 is primarily generated by recombination,

$$CF_3+F \xrightarrow{M} CF_4. \tag{13}$$

The rate coefficient for this process is strongly dependent on gas temperature and pressure. At 150 mTorr, the rate coefficient is (300–1000 K)[35]

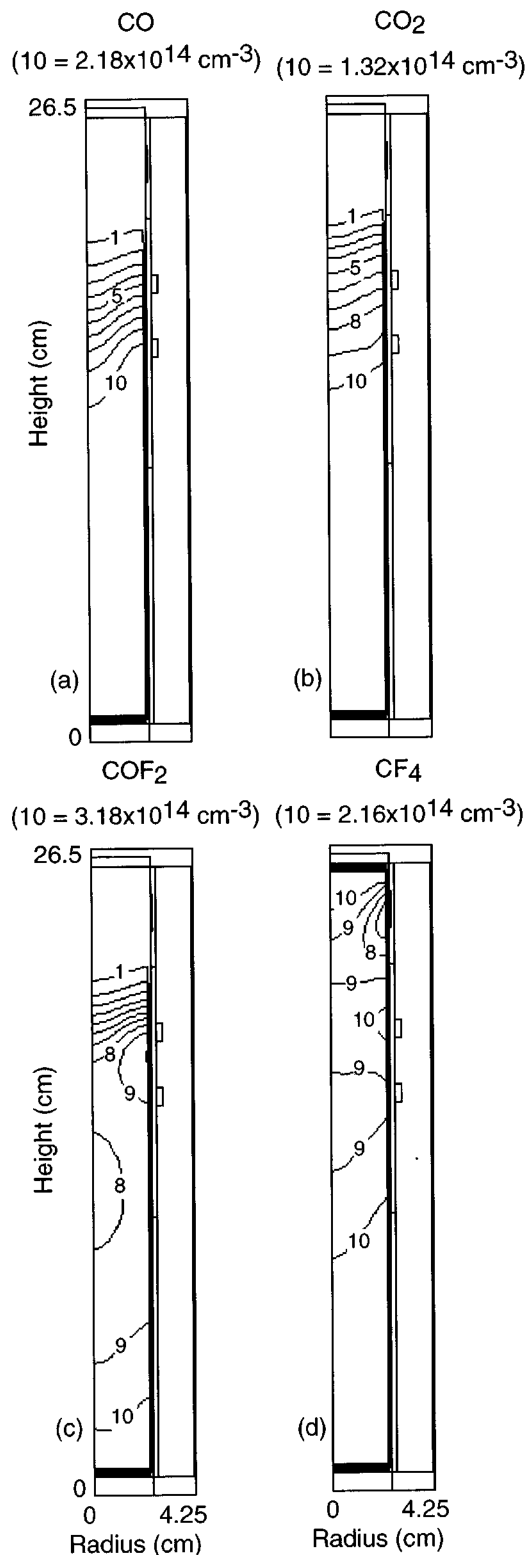

FIG. 14. Species densities for the baseline case of the plasma burn-box using O_2 as an additive. (a) CO, (b) CO_2, (c) COF_2, and (d) CF_4. Oxidation products are generated as the effluent passes through the plasma zone. Production of CF_4 occurs throughout the reactor. The contours are labeled by their relative magnitudes with the maximum values noted at the top of each figure.

TABLE IV. Abatement of species, primary products, and W-value of C_xF_y for the standard cases using O_2, H_2, or H_2O as additives.

			Initial-final
	Fractional abatement[a] for additives		Initial
Species	O_2	H_2	H_2O
C_2F_6	0.53	0.54	0.73
C_2F_5	>0.99	−0.47	0.37
C_2F_4	>0.99	−2.71	−0.31
C_2F_3	>0.99	0.22	0.35
CF_4	−1.4	0.23	0.04
CF_3	>0.99	0.96	0.98
CF_2	>0.99	−0.42	0.05
Products	COF_2, CO, CO_2, F, F_2	HF,CF,C	HF, COF_2, CO, CF, C, CO_2
η of all C_xF_y	0.54	0.42	0.65
W-value of C_xF_y eV	124.9	159.8	119.3

[a]Total abatement has value 1.0. Negative values of abatement denotes net production of that species.

$$k_{14}=4.9\times10^{-9}\left(\frac{T_g}{300}\right)^{-7.84}\exp\left(-\frac{1876.4}{T_g}\right)\text{cm}^{-3}\,\text{s}^{-1}. \quad (14)$$

The rate coefficient decreases by a factor of 4.5 by increasing the temperature from 300 K ($k=9.42\times10^{-12}\,\text{cm}^3\,\text{s}^{-1}$) to 500 K ($k=2.09\times10^{-12}\,\text{cm}^3\,\text{s}^{-1}$) and a factor of 158 with a temperature increase to 1000 K ($k=5.97\times10^{-14}\,\text{cm}^3\,\text{s}^{-1}$). Therefore, the generation of CF_4 could be reduced if the gas temperature is increased. For the base case, the wall temperature is fixed at 400 K, resulting in a mean gas temperature in the burn-box of ≈500 K at which the rate coefficient for CF_4 formation is still large. By increasing the wall temperature, the bulk gas temperature increases and the CF_4 in the exhaust decreases. This trend is shown in Fig. 15. The remaining C_2F_6 also decreases as the wall, gas and electron temperatures increase (and gas densities decrease) due to more favorable overlap of the region of high power deposition with the flow field of the C_2F_6. For example, the electron density shifts toward the center of the reactor due to the lower gas density.

The abatement of C_2F_6 and the generation of CF_4 are shown in Fig. 16 as a function of power and injected O_2 for the output effluent of the base case. [These results were obtained by performing a design of experiments and using a quadratic model (with cross terms) to fit the results to a response surface. A portion of the curvature of the surfaces results from the fit.] C_2F_6 abatement increases with increasing power and O_2 injection since there is more dissociation of O_2 and more subsequent reactions of O [and $O(^1D)$] with CF_x radicals. At low injected O_2, CF_4 generation increases with increasing power since much of the CF_3 produced by the dissociation of C_2F_6 is converted to CF_4 instead of reacting with oxygen radicals. At higher amounts of injected O_2, CF_4 generation decreases with increasing power since the CF_3 from the dissociation of C_2F_6 and other C_xF_y is rapidly converted to COF_2 in the oxygen radical-rich environment.

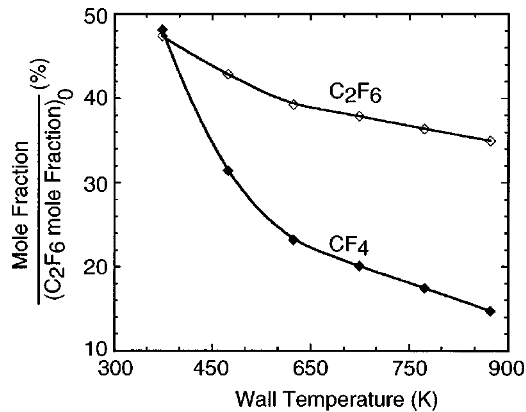

FIG. 15. C_2F_6 and CF_4 in the output stream (normalized by their input values) as a function of wall temperature for the baseline case of the plasma burn-box using O_2 as an additive. Increasing wall and gas temperature reduces the rate of CF_4 recombination.

The transition to low CF_4 generation occurs at about 90 sccm of injected O_2. These trends generally agree with Hartz *et al.*[8]

The abatement efficiency η is defined as the sum of the output flow rate of C_xF_y species weighted by the number of F atoms divided by the input flow rate,

$$\eta = 1 - \frac{\Sigma_i [f_i(C_xF_y)y]_{\mathrm{output}}}{\Sigma_i [f_i(C_xF_y)y]_{\mathrm{input}}}, \tag{15}$$

where f_i is the flow of the ith C_xF_y species in sccm. We again prejudice the calculation of efficiency by assuming that larger C_xF_y are "less good." η and the W-value for destruction of C_xF_y are shown in Fig. 17 for the conditions of Fig. 16. η increases with increasing power deposition and the amount of injected O_2 due to there being more CF_x radical and O atom generation. However, the W-value increases (lower power efficiency) with increasing power deposition (and particularly so at lower O_2 injection) since at higher power deposition more power is expended to further dissociate the products (e.g., COF_2 and CO_2).

C. H_2 as an additive for PFC abatement

In this subsection, we investigate H_2 as an additive gas for PFC abatement. Electron impact dissociation of H_2 generates H which in turn becomes the primary species for abating CF_x radicals. The dominant abatement reactions are[34,53]

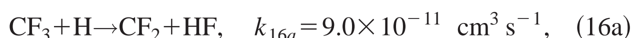

$$CF_3 + H \rightarrow CF_2 + HF, \quad k_{16a} = 9.0 \times 10^{-11}\ \mathrm{cm^3\,s^{-1}}, \tag{16a}$$

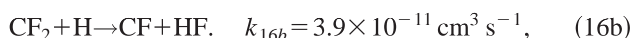

$$CF_2 + H \rightarrow CF + HF. \quad k_{16b} = 3.9 \times 10^{-11}\ \mathrm{cm^3\,s^{-1}}, \tag{16b}$$

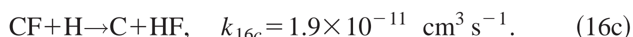

$$CF + H \rightarrow C + HF, \quad k_{16c} = 1.9 \times 10^{-11}\ \mathrm{cm^3\,s^{-1}}. \tag{16c}$$

In mixtures containing H_2, another significant process is the reaction between H_2 and F,[34]

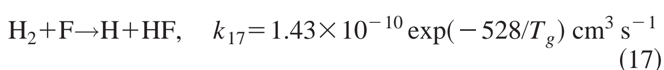

$$H_2 + F \rightarrow H + HF, \quad k_{17} = 1.43 \times 10^{-10} \exp(-528/T_g)\ \mathrm{cm^3\,s^{-1}} \tag{17}$$

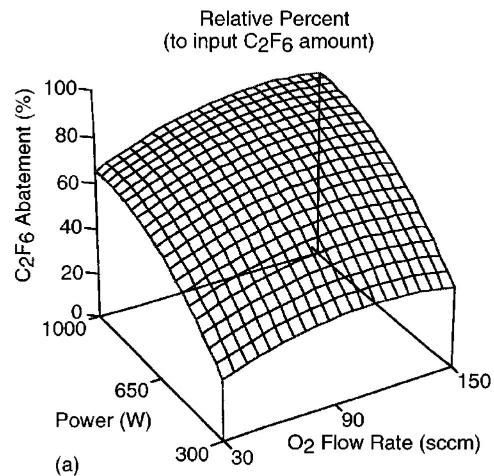

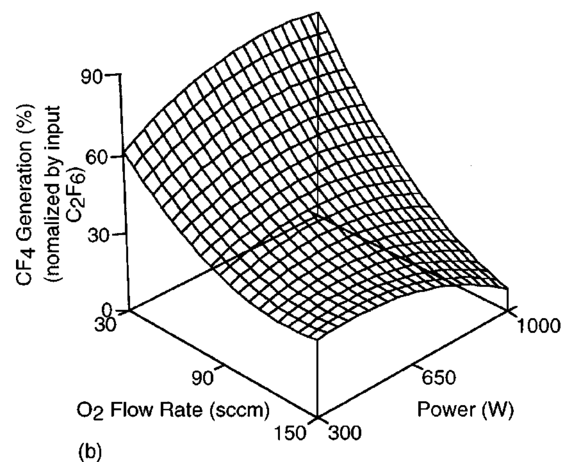

FIG. 16. Consumption of C_2F_6 and formation of CF_4 as a function of power and injected O_2 in the plasma burn-box. (a) Abatement of C_2F_6 and (b) generation of CF_4 normalized by the input C_2F_6 flow rate. (These figures are the output of a design-of-experiments whose response surface was fitted with a quadratic with cross terms. Some curvature of the surface results from the numerical fitting. Note that the independent variables have different orientations to obtain a better view angle.) CF_4 generation is most problematic at high powers and low oxygen flow rates.

which can substantially reduce the F atom density. The decrease in higher order CF_x radicals and the reduction in the availability of free fluorine further reduce the production of PFCs by reassociation, particularly so for CF_4.

The standard case is the same as that for using O_2 except that H_2 is injected at 150 sccm instead of oxygen. HF is the major product (mole fraction of 0.49) leaving the burn-box with there being lesser amounts of CF (0.094), C (0.074), and CF_2(0.041). The higher mole fractions of CF and CF_2 in the exhaust gas compared to using O_2 are due in part to there being insufficient H to reduce them to C. C_2F_6 and CF_3, the two primary C_xF_y species in the etching reactor effluent, are abated by 54.7% and 95.5%, respectively. (See Table IV for other C_xF_y species.) The CF_4 mole fraction, which is increased by 240% when using O_2 as an additive, is reduced by 23.5%. However, there is a significant increase in the amount of C_2F_4 (by a factor 2.4) due to the relatively high concen-

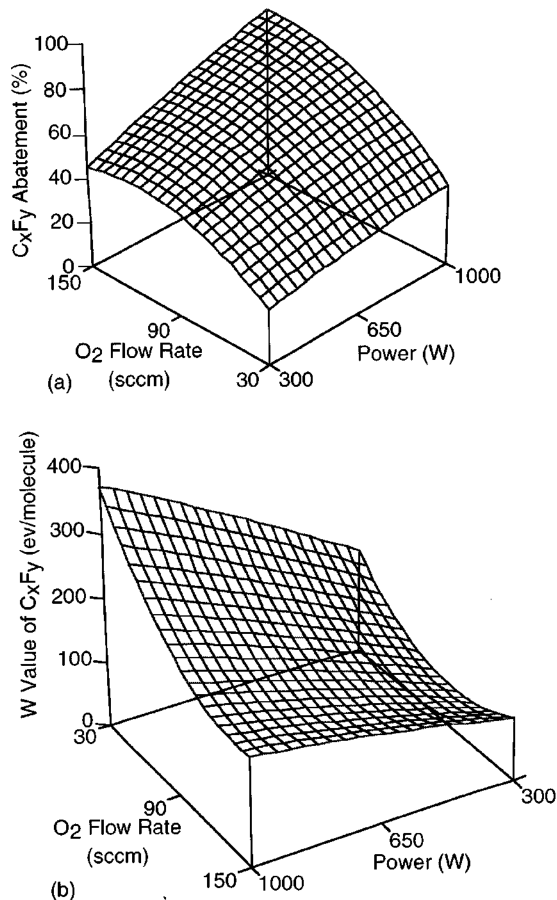

FIG. 17. Efficiencies for removal or conversion of all C_xF_y as a function of power and injected O_2 in the plasma burn-box. (a) Fractional C_xF_y abatement and (b) *W*-value for C_xF_y abatement. (Note that the independent variables have different orientations to obtain a better view angle.) Although abatement maximizes at high power and high oxygen flow rate, the efficiency is low (high *W*-value).

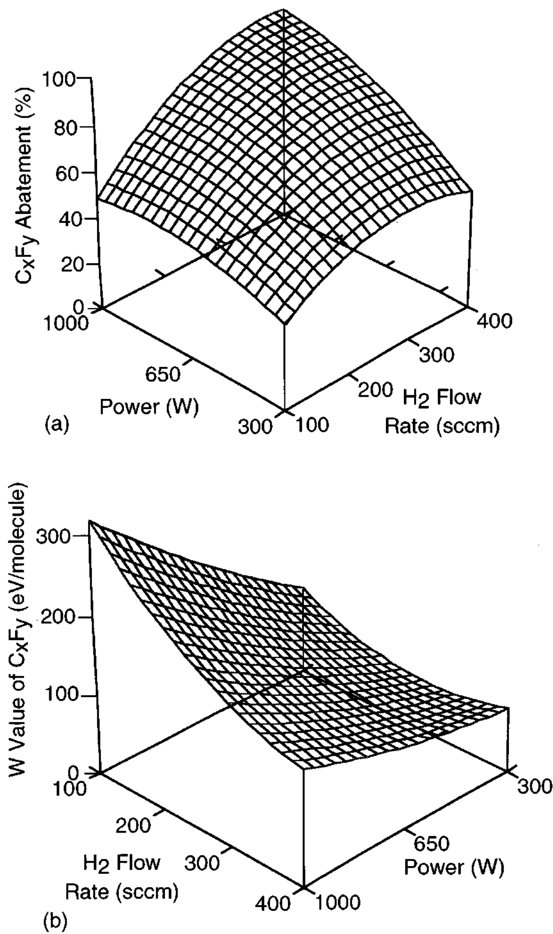

FIG. 18. Efficiencies for abatement of all C_xF_y as a function of power and injected H_2 in the plasma burn-box. (a) Fractional C_xF_y abatement and (b) *W*-value for C_xF_y. (Note that the independent variables have different orientations for to obtain a better view angle.)

tration of CF_2. C_2F_4 is still, however, a small mole fraction (<1%) in the exhaust.

The abatement efficiency η and *W*-value for C_xF_y as a function of power deposition and the amount of injected H_2 are shown in Fig. 18. Note that we chose a larger input of H_2 compared to the DOE using O_2 since three H_2 molecules are needed to remove all the F atoms in a C_2F_6 molecule. Only a single O_2 molecule is needed to oxidize a C_2F_6 if the oxidation product is CO or COF_2, and two O_2 molecules are required if the oxidation product is CO_2. At high power and high H_2 feed, almost all of the C and F atoms which are initially bound in C_xF_y species are converted to C and HF. As a consequence, η approaches 100%. As with using O_2 as an additive, increasing power deposition also increases the *W*-value of C_xF_y (less efficient).

D. H_2O as an additive for PFC abatement

H_2O is another promising additive for abating PFCs.[11] When using H_2O, electron impact dissociation produces O, H, and OH radicals. As discussed above, H and O are precursors for PFC remediation, however, OH can also remediate PFCs by both oxidizing CF_x and preventing its reassociation to make CF_4,[34]

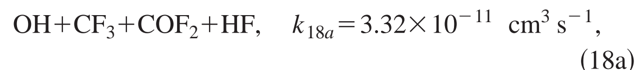

$$OH+CF_3+COF_2+HF, \quad k_{18a}=3.32\times10^{-11}\ cm^3\,s^{-1}, \tag{18a}$$

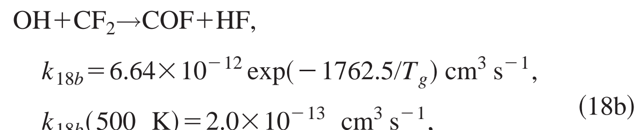

$$OH+CF_2\rightarrow COF+HF,$$
$$k_{18b}=6.64\times10^{-12}\exp(-1762.5/T_g)\ cm^3\,s^{-1},$$
$$k_{18b}(500\ K)=2.0\times10^{-13}\ cm^3\,s^{-1}, \tag{18b}$$

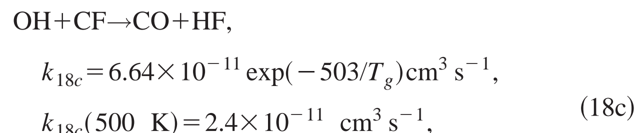

$$OH+CF\rightarrow CO+HF,$$
$$k_{18c}=6.64\times10^{-11}\exp(-503/T_g) cm^3\,s^{-1},$$
$$k_{18c}(500\ K)=2.4\times10^{-11}\ cm^3\,s^{-1}, \tag{18c}$$

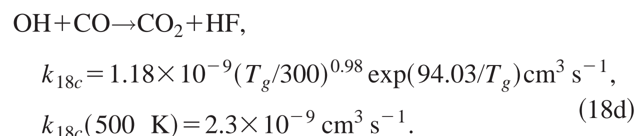

$$OH+CO\rightarrow CO_2+HF,$$
$$k_{18c}=1.18\times10^{-9}(T_g/300)^{0.98}\exp(94.03/T_g) cm^3\,s^{-1},$$
$$k_{18c}(500\ K)=2.3\times10^{-9}\ cm^3\,s^{-1}. \tag{18d}$$

H_2O can also directly react with F, which acts as a sink to remove free fluorine atoms which might otherwise recombine to form CF_4.

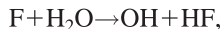

$$F+H_2O \rightarrow OH+HF,$$

$$k_{19}=1.11\times 10^{-11}(T_g/300)^{1.5}\ \mathrm{cm}^{-3}\,\mathrm{s}^{-1},$$

$$k_{19}(500\ \mathrm{K})=2.4\times 10^{-9}\ \mathrm{cm}^3\,\mathrm{s}^{-1}. \quad (19)$$

This reaction generates OH which is then available for further remediation, thereby forming a chain reaction.

To investigate H_2O as an additive, the base case was modeled using 150 sccm of water vapor. The results show that H_2O is more effective for PFC abatement than either O_2 or H_2, in agreement with experiments by Tonnis *et al.*[11] For example, the two major C_xF_y species in the etching effluent, C_2F_6 and CF_3, are abated by 73% and 98% without there being additional CF_4 generation. CF_4 (a minority C_xF_y species in the etching effluent) is reduced by 9.7%. Other C_xF_y species are also decreased to different extents as shown in Table IV. The exception is that there is a slight increase of C_2F_4. For the base case, the F atoms which were initially bound in all C_xF_y were converted to products in the following proportions: HF, 59.8%, and COF_2, 40%. Only traces of F are in other species (COF, F_2, FO, F, and CF_3O_2). The carbon atoms initially bound in C_xF_y were converted to products in the following proportions: COF_2, 63.3%, CO, 31.4%; C, 3.9%; and CO_2, 1.4%. At higher power and higher water vapor input, all C_xF_y can be decreased to low concentrations. For example, η and *W*-values for C_xF_y as a function of power and injected water vapor are shown in Fig. 19. High η is obtained at high powers with a large feed of H_2O. Low *W*-values (high efficiency) are obtained at high input H_2O flow rates with low power. These trends are similar to the cases using H_2 except for there being a higher efficiency and lower *W*-value.

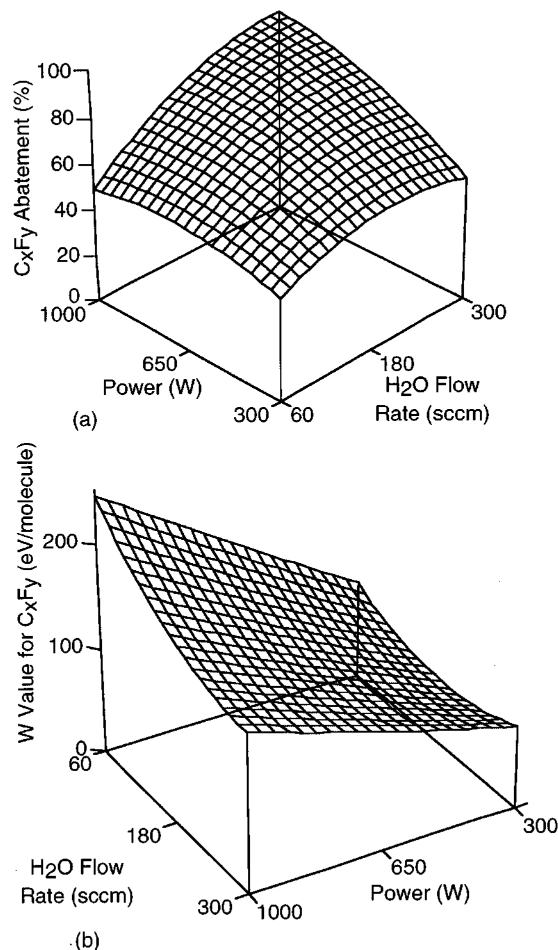

FIG. 19. Efficiencies for abatement of all C_xF_y as a function of power and injected H_2O in the plasma burn-box. (a) Fractional C_xF_y abatement and (b) *W*-value for C_xF_y. (Note that the independent variables have different orientations to obtain a better view angle.)

V. CONCLUDING REMARKS

Results from a computational investigation of the consumption and generation of PFCs in an ICP etching reactor for Ar/C_2F_6 and Ar/CF_4 gas mixtures and the abatement of the effluent in an ICP burn-box have been discussed. The model was validated by comparison to experiments by Sawin and Vitale[9] using C_2F_6/O_2 mixtures. C_2F_6 (or CF_4) consumption in the etching reactor is proportional to ICP power deposition, and inversely proportional to C_2F_6 mole fraction and total gas flow rate. We found a ceiling of 158 eV/molecule for consumption of C_2F_6 and 175 eV/molecule for CF_4 for our baseline cases, Ar/C_2F_6 (or Ar/CF_4) = 60/40 at 500 W power deposition. The generation of C_xF_y in the effluents of Ar/C_2F_6 gas mixtures is approximately twice that for Ar/CF_4 gas mixture under the same conditions. There is slightly more generation of F and F_2 for the CF_4 feedstock gas.

In general, CF_4 generation occurs during abatement of C_2F_6 using O_2 as an additive. This is especially true for high power with low O_2 input due to there being low concentrations of O and $O(^1D)$ atoms while there are large densities of F and CF_3. At high gas temperatures, there is a significant reduction of CF_4 generation since the rate coefficient for recombination of CF_3 and F decreases. The major oxidation products are COF_2, CO, and CO_2. H_2 can be used as an abatement additive without producing CF_4 since hydrogen reacts rapidly with free fluorine which would otherwise reassociate with CF_x to form CF_4. F and C atoms initially contained in C_xF_y are converted to HF and C. Generation of C atoms could be problematic due to their deposition on surfaces. It was also shown that H_2O is a promising and efficient abatement additive gas since it is a source of oxygen, hydrogen and hydroxyl radicals, produced in beneficial mole fractions. The primary products of abatement using water vapor are HF, CO, COF_2 with small amounts of C and CO_2.

ACKNOWLEDGMENTS

This work was supported by the Semiconductor Research Corporation, Applied Materials Inc., and LAM Research. The authors thank D. Burgess for performing calculations of rate coefficients for them.

[1]A. Tserspi, W. Schwarzenbach, J. Derouard, and N. Sadeghi, J. Vac. Sci. Technol. A **15**, 3120 (1997).

[2]M. A. Sobolewski, J. G. Langan, and B. S. Felker, J. Vac. Sci. Technol. B **16**, 173 (1998).
[3]*Plasma Etching: An Introduction*, edited by D. M. Manos and D. L. Flamm (Academic, San Diego, CA, 1989).
[4]T. E. F. M. Standaert, M. Schaepkens, N. R. Rueger, P. G. M. Sebel, G. S. Oehrlein, and J. M. Cook, J. Vac. Sci. Technol. A **16**, 239 (1998).
[5]L. Beu, P. T. Brown, J. Latt, J. U. Papp, T. Gilliland, T. Tamayo, J. Harrison, J. Davison, A. Cheng, J. Jewett, and W. Worth, Current State of Technology: Perfluorocompound (PFC) Emissions Reduction, SEMATECH Technology Transfer No. 98053508A-TR, 1998.
[6]S. P. Sun, D. Bennett, L. Zazzera, and W. Reagen, Semicond. Int., February 1998, p. 85.
[7]V. Mohindra, H. Chae, H. H. Sawin, and M. T. Mocella, IEEE Trans. Semicond. Manuf. **10**, 399 (1997).
[8]C. L. Hartz, J. W. Bevaan, M. W. Jackson, and B. A. Wofford, Environ. Sci. Technol. **32**, 682 (1998).
[9]H. H. Sawin and S. A. Vitale, 51st Gaseous Electronics Conference, Maui, Hawaii, Oct. 1998.
[10]A. Fiala, M. Kiehlbauch, S. Mahnovski, and D. B. Graves, J. Appl. Phys. **86**, 152 (1999).
[11]E. J. Tonnis, V. Vartanian, L. Beu, T. Lii, R. Jewett, and D. Graves, Evaluation of a Litmas ''Blue'' Point-of-Use (POU) Plasma Abatement Device for Perfluorocompound (PFC) Destruction, SEMATECH Technology Transfer No. 98123605A-TR, 1998.
[12]S. Rauf and M. J. Kushner, J. Appl. Phys. **82**, 2805 (1997).
[13]M. J. Grapperhaus, Z. Krivokapic, and M. J. Kushner, J. Appl. Phys. **83**, 35 (1998).
[14]R. A. Svehla, NASA Technical Report R-132, 1962.
[15]M. Mitchner and C. H. Kruger, Jr., *Partially Ionized Gases* (Wiley, New York, 1973), p. 93.
[16]E. H. Kennard, *Kinetic Theory of Gases* (McGraw–Hill, New York, 1938).
[17]Y. Sone, T. Ohwada, and K. Aoki, Phys. Fluids A **1**, 363 (1989).
[18]S. K. Loyalka, Physica A **163**, 813 (1990).
[19]L. B. Thomas, in *Fundamentals of Gas-Surface Interactions*, edited by H. Saltsburg, J. N. Smith, and M. Rogers (Academic, New York, 1967), pp. 346–369.
[20]P. A. Thompson, *Compressible Fluid Dynamics* (McGraw–Hill, New York, 1972), Section 2.5.
[21]K. Tachibana, Phys. Rev. A **34**, 1007 (1986).
[22]D. Rapp and P. Englander-Golden, J. Chem. Phys. **43**, 1464 (1965).
[23]R. H. McFarland and J. D. Kinney, Phys. Rev. **137**, A1058 (1965).
[24]R. A. Bonham, Jpn. J. Appl. Phys., Part 1 **33**, 4157 (1994).
[25]M. Hayashi, in *Gaseous Dielectrics V*, edited by L. G. Christophorou and D. W. Bouldin (Pergamon, New York, 1987).
[26]M. Hayashi and T. Nimura, J. Appl. Phys. **54**, 4879 (1983).
[27]E. Fisher, M. E. Weber, and P. B. Armentrout, J. Chem. Phys. **76**, 4932 (1982).
[28]G. K. Jarvis, C. A. Mayhew, R. P. Tuckett, J. Phys. Chem. **100**, 17166 (1996).
[29]P. K. Leichner and R. J. Ericson, Phys. Rev. A **9**, 251 (1974).
[30]J. E. Velazco, J. H. Koltz, and D. W. Sester, J. Chem. Phys. **65**, 3468 (1976).
[31]R. E. Olson, J. R. Peterson, and J. Moseley, J. Chem. Phys. **53**, 3391 (1971).
[32]E. L. Duman, N. P. Tishchenko, and I. P. Shmatov, Dokl. Phys. Chem. **295**, 5 (1987).
[33]I. C. Plumb and K. R. Ryan, Plasma Chem. Plasma Process. **6**, 205 (1986).
[34]D. R. F. Burgess, Jr., M. R. Zachariah, W. Tsang, and P. R. Westmoreland, Prog. Energy Combust. Sci. **21**, 453 (1996).
[35]D. R. F. Burgess, Jr., National Institute of Standards and Technology (private communication).
[36]A. V. Phelps, JILA Information Center Report No. 28, University of Colorado, 1985.
[37]E. Krishnakumar and S. K. Srivastava, Int. J. Mass Spectrom. Ion Processes **113**, 1 (1992).
[38]R. R. Laher and F. R. Gilmore, J. Phys. Chem. Ref. Data **19**, 277 (1990).
[39]M. Hayashi and T. Nimura, J. Appl. Phys. **54**, 4879 (1983).
[40]V. McKoy, C. Winstead, and W. L. Morgan, ''Data compilation for Plasma Chemistries,'' Sematech Technology Transfer Document 970432274A-TR, August 1997.
[41]J. J. Lowke, A. V. Phelps, and B. W. Irwin, J. Appl. Phys. **44**, 4664 (1973).
[42]M. Hayashi, J. Phys. Colloq. **C7**, Suppl. 40, C7/45 (1979).
[43]M. Hayashi, in *Swarm Studies And Inelastic Electron-Molecular Collisions*, edited by L. C. Pitchford, B. V. Mckoy, A. Chutjian, and S. Trajmar (Springer, New York, 1987), p. 187.
[44]B. R. Rowe, F. Vallee, J. L. Queffelec, J. C. Gomet, and M. Morlais, J. Phys. Chem. **88**, 845 (1988).
[45]J. B. A. Mitchell, Phys. Rep. **186**, 215 (1990).
[46]D. L. Parent, R. Derai, G. Mauclaire, M. Heninger, R. Marx, M. E. Rincon, A. O'Keefe, and M. T. Bowers, Chem. Phys. Lett. **117**, 127 (1985).
[47]P. Gaucherel, J. Mol. Spectrosc. **25**, 211 (1977).
[48]L. G. Piper, J. E. Velazco, and D. W. Setser, J. Chem. Phys. **59**, 4932 (1973).
[49]Y. Ikezoe, S. Matsuoka, M. Takebe, and A. Viggiano, *Gas-phase Ion-Molecule Reaction Rate Constants Through 1986* (Maruzen, Tokyo, 1987).
[50]J. C. Person and D. O. Ham, Radiat. Phys. Chem. **31**, 1 (1988).
[51]D. L. Baulch, C. J. Cobos, R. A. Cox, C. Esser, P. Frank, T. Just, J. A. Kerr, M. J. Pilling, J. Troe, R. W. Walker, and J. Warnatz, J. Phys. Chem. Ref. Data **21**, 411 (1992).
[52]W. Tsang and R. F. Hampson, J. Phys. Chem. Ref. Data **15**, 1087 (1986).
[53]C. Tsai and D. L. McFadden, J. Phys. Chem. **93**, 2471 (1989).
[54]D. Husain and L. J. Kirsch, Trans. Faraday Soc. **67**, 2025 (1971).
[55]R. Atkinson, D. L. Baulch, R. A. Cox, R. F. Hampson, J. A. Kerr, and J. Troe, J. Phys. Chem. Ref. Data **21**, 1125 (1992).
[56]C. D. Walther and H. G. Wagner, Ber. Bunsenges. Phys. Chem. **87**, 403 (1983).
[57]W. B. DeMore, D. M. Golden, R. F. Hampson, C. J. Howard, M. J. Kurylo, M. J. Molina, A. R. Ravishankara, and S. P. Sander, JPL Publ. **1**, 87 (1987).
[58]J. P. Burrows, D. I. Cliff, G. W. Harris, B. A. Thrush, and J. P. T. Wilkinson, Proc. R. Soc. London, Ser. A **368**, 463 (1980).
[59]L. C. Lee and T. G. Slanger, Geophys. Res. Lett. **6**, 165 (1979).
[60]E. R. Fisher and P. R. Armentrout, J. Phys. Chem. **95**, 6118 (1991).
[61]L. G. Christophorou, Contrib. Plasma Phys. **27**, 237 (1987).